Materials Today Bio 29 (2024) 101314

Contents lists available at ScienceDirect

Materials Today Bio

journal homepage: www.journals.elsevier.com/materials-today-bio

Engineering exosomes from fibroblast growth factor 1 pre-conditioned adipose-derived stem cells promote ischemic skin flaps survival by activating autophagy

Xuanlong Zhang [a,b], Xiaoqiong Jiang [b,d], Huiming Deng [b], Gaoxiang Yu [c], Ningning Yang [c], Abdullah Al Mamun [b], Feifei Lian [b], Tianling Chen [b], Haijuan Zhang [b], Yingying Lai [c], Jiayi Huang [b], Shi Xu [d], Fuman Cai [d], Xiaokun Li [a,b,**], Kailiang Zhou [c,***], Jian Xiao [a,b,c,*]

[a] Department of Wound Healing, The First Affiliated Hospital of Wenzhou Medical University, Wenzhou, 325015, China
[b] Oujiang Laboratory (Zhejiang Lab for Regenerative Medicine, Vision and Brain Health), School of Pharmaceutical Sciences, Wenzhou Medical University, Wenzhou, Zhejiang, 325035, China
[c] Department of Orthopaedics, The Second Affiliated Hospital and Yuying Children's Hospital of Wenzhou Medical University, Wenzhou, 325027, China
[d] College of Nursing, Wenzhou Medical University, Wenzhou, 325000, China

ARTICLE INFO

Keywords:
Exosomes
Fibroblast growth factor 1
Autophagy
Skin flaps
GPR137

ABSTRACT

Background: The recovery of ischemic skin flaps is a major concern in clinical settings. The purpose of this study is to evaluate the effects of engineered exosomes derived from FGF1 pre-conditioned adipose-derived stem cells (FEXO) on ischemic skin flaps.

Method: 6 patients who suffered from pressure ulcer at stage 4 and underwent skin flaps surgery were recruited in this study to screen the potential targets of ischemic skin flaps in FGF family. FGF1 was co-incubated with adipose stem cells, and ultracentrifugation was applied to extract FEXO. Transcriptome sequencing analysis was used to determine the most effective microRNA in FEXO. Animal skin flaps models were established in our study to verify the effects of FEXO. Immunofluorescence (IF), western blotting (WB) and other molecular strategy were used to evaluate the effects and mechanism of FEXO.

Results: FGF1 was expected to be the therapeutic and diagnostic target of ischemic skin flaps, but there is still some deficiency in rescuing skin flaps. FEXO significantly improved the viability of RPSFs and endothelial cells by inhibiting oxidative stress and alleviating apoptosis and pyroptosis through augmenting autophagy flux. In addition, FEXO inhibited the over-activated inflammation responses. Transcriptome sequencing analysis showed that miR-183-5p was significantly elevated in FEXO, and inhibiting miR-183-5p resulted in impaired protective effects of autophagy in skin flaps. The exosomal miR-183-5p markedly enhanced cell viability, inhibited oxidative stress and alleviated apoptosis and pyroptosis in endothelial cells by targeting GPR137 through Pi3k/Akt/mTOR pathway, indicating that GPR137 could also be a therapeutic target of ischemic skin flap. It was also notabale that FGF1 increased the number of exosomes by upregulating VAMP3, which may be a promising strategy for clinical translation.

Conclusion: FEXO markedly improved the survivial rate of ischemic skin flaps through miR-183-5p/GPR137/Pi3k/Akt/mTOR axis, which would be a promising strategy to rescue ischemic skin flaps.

* Corresponding author. Oujiang Laboratory (Zhejiang Lab for Regenerative Medicine, Vision and Brain Health), School of Pharmaceutical Sciences, Wenzhou Medical University, Wenzhou, Zhejiang, 325035, China.
** Corresponding author. Oujiang Laboratory (Zhejiang Lab for Regenerative Medicine, Vision and Brain Health), School of Pharmaceutical Sciences, Wenzhou Medical University, Wenzhou, Zhejiang, 325035, China.
*** Corresponding author.
E-mail addresses: profxiaokunli@163.com (X. Li), zhoukailiang@wmu.edu.cn (K. Zhou), xfxj2000@126.com (J. Xiao).

https://doi.org/10.1016/j.mtbio.2024.101314
Received 2 September 2024; Received in revised form 16 October 2024; Accepted 25 October 2024
Available online 26 October 2024

Abbreviations

FGF1	Fibroblast growth factor 1
FGF2	Fibroblast growth factor 2
FGF7	Fibroblast growth factor 7
FGF9	Fibroblast growth factor 9
FGF11	Fibroblast growth factor 11
FGF12	Fibroblast growth factor 12
FGF14	Fibroblast growth factor 14
FGF16	Fibroblast growth factor 16
FGF18	Fibroblast growth factor 18
FGF21	Fibroblast growth factor 21
FGFR1	Fibroblast growth factor receptor 1
FGFR2	Fibroblast growth factor receptor 2
FGFR4	Fibroblast growth factor receptor 4
EXO	Exosomes from adipose-derived stem cells
FEXO	Exosomes from FGF1-preconditioned adipose-derived stem cells
D1	The first day post-surgery
D3	The third day post-surgery
D5	The fifth day post-surgery
D7	The seventh day post-surgery
GPRs	G protein-coupled receptors
GPR137	G protein-coupled receptor 137
NLRP3	NLR family pyrin domain containing 3
GSDMD-N:	Gasdermin D-N
Cleaved Caspase-1	CC1
CYC	Cytochrome *c*
ADSCs	Adipose-derived stem cells
F- ADSCs	FGF1-preconditioned adipose-derived stem cells
OGD	Oxygen glucose deprivation
AGEs	Advanced glycation end-products
RPSFs	Random-pattern skin flaps
LDBF	Laser Doppler blood flow
mTOR	Mammalian target of rapamycin
LC3	Microtubule-associated protein 1 light chain 3
p62/SQSTM1	Sequestosome 1
VAMP1	Vesicle associated membrane protein 1
VAMP2	Vesicle associated membrane protein 2
VAMP3	Vesicle associated membrane protein 3
VAMP5	Vesicle associated membrane protein 5
VAMP8	Vesicle associated membrane protein 8
3-MA	3-methyladenine
PETCM	alpha-(trichloromethyl)-4-pyridine-ethanol
DMNQ	2,3-dimethoxy-1,4-naphthoquinone

1. Background

Skin flaps surgery are convenient methods in clinical practice for reconstructing skin defects induced by trauma and severe burns [1–3]. As representative of ischemic skin flaps, random-pattern skin flaps (RPSFs) are commonly applied in clinics due to the convenience and effectiveness. However, the insufficient blood perfusion in tissue always leads to ischemia on the distal part of skin flaps [4,5]. RPSFs cannot be extended in the case of excessive ischemic necrosis, resulting in a limitation in the challenge of massive cutaneous defects. More complex procedures reconstructing complex skin defects are involved in the perforator skin flaps, free skin flaps and axial flaps, which usually cause extra damage to donor sites [6–8]. Although several physical and chemical approaches are used to rescue the ischemic skin flaps, the recovery of ischemic skin flaps is a still major concern in clinical settings. Especially for the wound caused by pressure ulcers at stage 4, skin flaps seems to be the one way to reconstruct the skin defects. Therefore, this study concentrated on discovering the potential target of ischemic RPSFs from pressure -injured patients and exploring a new strategy for alleviating ischemic skin flaps by using the mouse RPSFs model [9].

A series of injuries are associated with ischemia such as oxidative stress and programmed cell death including apoptosis and pyroptosis [10–12]. Pyroptosis is a form of programmed cell death characterized by triggering low-grade inflammation [13]. Inflammasomes formed from NLRP3 induce the self-cleavage of Caspase-1 into Cleaved Caspase-1 (CC-1) [14]. CC-1 activates GSDMD-N, resulting in membrane rupture and cell death [15]. Accumulating evidence indicates that ROS induces the damage of genetic materials and alters the membrane integrity of mitochondria, which further results in the release of CYC from mitochondria to function in the apoptosis pathway [16,17]. The cellular damage and ischemia-induced skin necrosis can be prevented by alleviating oxidative stress, apoptosis and pyroptosis.

The autophagic process protects a wide variety of stresses [18]. In addition, autophagy decomposes waste and excessive nutrients to maintain a balanced internal environment. Several experiments have shown that autophagy significantly facilitates cutaneous and soft tissue regeneration [19,20]. FGF1 was overexpressed in necrotic area of RPSFs on the seventh day post-surgery in both patients and mice, suggesting that FGF1 might protect necrotic skin flaps. Numerous studies have shown that FGF1 is unstable in severe environments, sensitive to proteases and prone to aggregates, leading to the reduction of half-life [21,22]. Previous studies have demonstrated that growth factors can induce immunogenic reactions in some individuals [23]. In addition , several researcher also have pointed out the deficiency of FGF1 rescuing skin flaps [24]. Intriguingly, studies have shown that stem cells have the potentials to soft tissue and vascular regeneration [25,26]. The application of stem cells in clinics was limited due to the risks of differentiation, tumor formation and immunogenicity [27,28]. Exosomes are extracellular vesicles containing proteins, miRNAs, large non-coding RNAs, mRNAs and other genetic material, which show more effective than stem cell transplantation with greater safety [29,30].

This study demonstrated that exosomes isolated from FGF1 preconditioned adipose-derived stem cells (FEXO) significantly improved the survival of RPSFs. It was also found that FEXO restricted the activation of oxidative stress and suppressed pyroptosis and apoptosis by enhancing autophagy. More importantly, the findings from our study revealed that FGF1 facilitated the production of exosomes by upregulating VAMP3, which provides a new strategy for improving engineering techniques in the production of exosomes in the future.

2. Results

2.1. FGF1 might be a diagnostic and therapeutic target for ischemic random -pattern skin flaps

Six male patients who underwent reconstructive surgery of RPSFs resulting from sacrococcygeal pressure ulcers and three of them showed partial necrosis in skin flaps were collected (Table 1) (supplementary data). Transcriptome sequencing analysis was used to discover the differences of genes expression between necrotic area and survived area of skin flaps in patients (Fig. 1 A-B) and GO analysis indicated that several pathway were involved in skin flaps necrosis, including regulation of fibroblasts growth factors signaling and production, autophagy and apoptosis etc (Fig. 1. C). In order to explore the potential targets of FGFs in skin flaps, transcriptome sequencing analysis of FGFs family was further executed, and several upregulated FGFs were detected in patients necrotic skin flaps (Fig. 1. D). It was notable that mRNAs level of FGFs were increased in necrotic area of mice skin flaps, expecially for

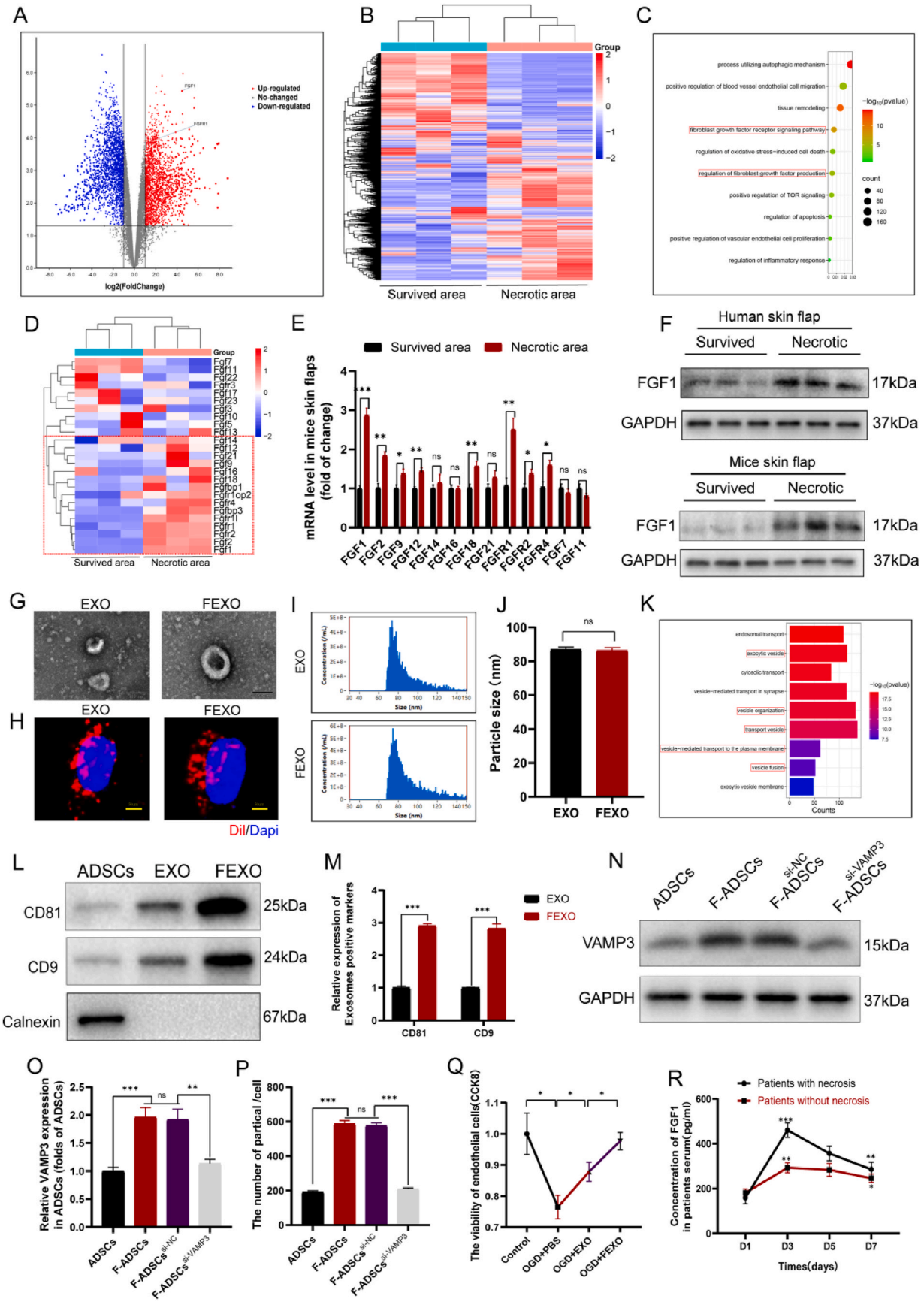

(caption on next page)

Fig. 1. The expression of FGF1 and the identification and comparison of EXO and FEXO. (A) The volcano plot of different mRNAs of human skin flaps. (B) The transcriptome sequencing analysis of human skin flaps. (C) Representative signaling pathways of genes targeted by significantly differential mRNAs according to GO analysis. (D) The transcriptome sequencing analysis of FGFs family in human skin flaps, and the upregulated FGFs in necrotic area were labeled by red rectangle. (E) qPCR result of FGF1, FGF2, FGF9, FGF12, FGF14, FGF16, FGF18, FGF21, FGFR1, FGFR2, FGFR4,FGF7 and FGF11 in necrotic and survived area of mice skin flaps (n = 5). (F) The western blot images of FGF1 in human skin flaps and mice skin flaps. (G)The transmission electron microscopy image of EXO and FEXO. (H) Uptake of Dil-labeled EXO and FEXO into OGD endothelial cells. (I) The particle distribution of EXO and FEXO by NTA analysis. (J) Particle sizes of EXO and FEXO were analyzed (n = 3). (K) Representative signaling pathways of genes targeted by significantly differential microRNAs according to GO analysis of FEXO versus EXO. (L) Western blot analysis of biomarkers of EXO and FEXO. Extracellular vesicle positive marker CD81 and CD9 and negative control calnexin. The gels have been run under the same experimental conditions, and cropped blots were used here. (M) The density value of the proteins previously described in each group (n = 3). (N) The western blotting of VAMP3 in ADSCs, F-ADSCs, F-ADSCs$^{si\text{-}NC}$, F-ADSCs$^{si\text{-}VAMP3}$. The gels have been run under the same experimental conditions, and cropped blots were used here. (O) The density value of VAMP3 in each group (n = 3). (P) The number of particles produced by each ADSC was analyzed by NTA in ADSC and F-ADSC groups (n = 5). (Q) The viability of OGD endothelial cells by CCK8 analysis (n = 5). (R) The Elisa results of FGF1 in patients serum (n = 3). * stands for $P < 0.05$, ** stands for $P < 0.01$, *** stands for $P < 0.001$, ns stands for not significant.

FGF1, and FGFR1 (Fig. 1. E). The WB assays further validated that FGF1 was similarly enhanced in both patients and mice necrotic area skin flaps (Fig. 1. F/SF 1. E-F). The Elisa assays were also performed to detect the concentration of FGF1 in serum of patients with or without necrosis in RPSFs (Fig. 1. R). It was notable that the level of FGF1 in all patients was elevated after RPSFs surgery. The patients with apparent necrosis displayed higher peak at D3 after surgery, with a gradual decrease of FGF1 in the rest of 4 days. These evidence indicated that FGF1 would be a new index to predict potential necrosis after RPSFs surgery. In addition, FGF1 might also be a therapeutic target in skin flaps, which was further verified by our following study (Fig. 2 A, D). However, previous studies have mentioned deficiencies of FGF1 and its unsatisfactory effects in skin flaps regeneration [31]. Exosomes have already possess therapeutic value for cutaneous regeneration. Therefore, we aimed to establish a new strategy to rescue ischemic RPSFs with the combination of exosomes with FGF1.

2.2. Identification and comparison of EXO and FEXO

Adipose-derived stem cells (ADSCs) were cultured and divided into two groups. FGF1 were co-cultured with ADSCs for 48 h and collected the culture medium for further exosome isolation. In Fig. 1G, EXO and FEXO showed a cup-shaped or sphere-shaped morphology under transmission electron microscopy (TEM). The images from fluorescence microscopy indicated that Dil-labeled EXO and FEXO were found within the cytoplasm and mostly surrounding the nucleus of target endothelial cells (Fig. 1 H). Intriguingly, the nanoparticles of EXO and FEXO exhibited similar tracking characteristics (Fig. 1 I-J). EXO and FEXO were then analyzed using western blot assay to detect the extracellular vesicle surface markers (CD81 and CD9) and the absence of the negative extracellular vesicle marker calnexin (Fig. 1 L-M). Western blot assay showed the expression of exosome-positive markers in FEXO were elevated nearly 3- fold, indicating that more exosomes were generated from FGF1 pre-conditioned ADSCs. The GO analysis of FEXO versus EXO indicated that vesicles organization, fusion and transportation related pathway were significantly upregulated after treatment with FGF1 (Fig. 1. K). In addition, the number of exosomes produced by single F-ADSC was increased nearly 3- fold than that produced by single ADSC (Fig. 1. P). This phenomenon indicated that more nanoparticles were generated from FEXO group than in EXO group. NTA was further used to analyze the number of exosomes excreted by ADSCs. It was reported that VAMP3 play an important role in extracellular vesicles (EVs) transporting and membrane trafficking of cells [32]. Therefore, experiments further investigated whether VAMP3 played an important role in F-ADSCs EVs transportation. The mRNA level of potential VAMPs (VAMP1, VAMP2, VAMP3, VAMP5 and VAMP8) that influence exosomes secretion in ADSCs were further analyzed **(SF 1. T)**. It turned out that the VAMP3 was most significantly upregulated. FGF1 increased the expression of VAMP3. After inhibition of VAMP3, the number of exosomes from ADSCs was significantly decreased (Fig. 1 N-P). The phenomenon indicated that FGF1 enhancing exosomes production was regulated by VAMP3, providing a new strategy for engineering exosomes.

2.3. FEXO enhanced angiogenesis and autophagy, inhibited oxidative stress and alleviated apoptosis and pyroptosis in random-pattern skin flaps

RPSF models were stablished on the dorsum of mice to investigate the effects of FGF1. FGF1 was injected into the skin flaps in the middle of the surgery at different concentration (**SF 1. C)**. Although FGF1 improved the survival rate of skin flaps at 15ug/ml, its therapeutic effect seemed to be limited as the dosage increased (**SF 1. D**). EXO was subsequently applied to verify its efficacy on skin flaps. The necrotic area was partially decreased at 100ug/ml, but more severe injuries were observed at higher concentration (**SF 1. A-B**). In order to solve the deficiencies of the clinical proven drugs, FEXO (the combination of EXO and FGF1) was engineered to rescue RPSFs.

Compared to the PBS group, the EXO and FGF1 groups showed decreased necrotic areas and confined them to Area III (Fig. 2 A, D). The laser Doppler blood flow assay (LDBF) was performed to determine the level of blood flow in skin flaps (Fig. 2 B, E). Compared to PBS, EXO and FGF1, skin flaps treated with FEXO demonstrated the highest level of blood flow and survival rate. The relative temperatures of skin flaps were measured using an infrared thermal imager (Fig. 2. C). Intriguingly, a significant difference in relative temperature between the FEXO and the other three groups (Fig. 2. F).

It turned out that FEXO was more effective than FGF1 or EXO in terms of survival rate, blood flow and cutaneous temperature in RPSFs. Accordingly, the mechanism by which FEXO protects RPSFs were examined. Western blot were executed to determine the expression of proteins involved in angiogenesis (VEGF), autophagy (LC3B and p62) and pyroptosis (NLRP3, GSDMD-N and CC1) in Area II of skin flaps (Fig. 2. G/SF 2.A). It was demonstrated that EXO and FEXO down-regulated the expression level of pyroptosis-related proteins and enhanced angiogenesis and autophagy flux in skin flaps. The results from immunofluorescence (IF) staining indicated that EXO and FEXO augmented the number of CD31/EMCN double-positive blood vessels in skin flaps (Fig. 2. H/SF 2.B). And the number of infiltrated $CD4^+$/$Foxp3^+$ Treg cells was increased by FEXO (Fig. 2. I/SF 2. C). In addition, the decrement of M1 macrophages was detected in EXO and FEXO group (Fig. 2. J/SF 2. D). Moreover, the results revealed that EXO and FEXO remarkably suppressed the activity of Caspase-1 in skin flaps (**SF 2. E**). DHE staining, TUNEL staining and CYC IF analysis (**SF 1. G-I**) were performed to determine oxidation and apoptosis levels. Taken together, these findings indicated that FEXO and EXO obstructed the activation of oxidative stress and alleviated apoptosis in the skin flaps (**SF 1. M-O**).

2.4. FEXO enhanced autophagy and viability and alleviated pyroptosis in endothelial cells

The intensity of GSDMD-N and the punctuation of LC3B were detected using IF in OGD-induced endothelial cells. More importantly, the results showed that EXO and FEXO decreased the intensity of GSDMD-N (Fig. 3 A, C) and enhanced the number of activated LC3B

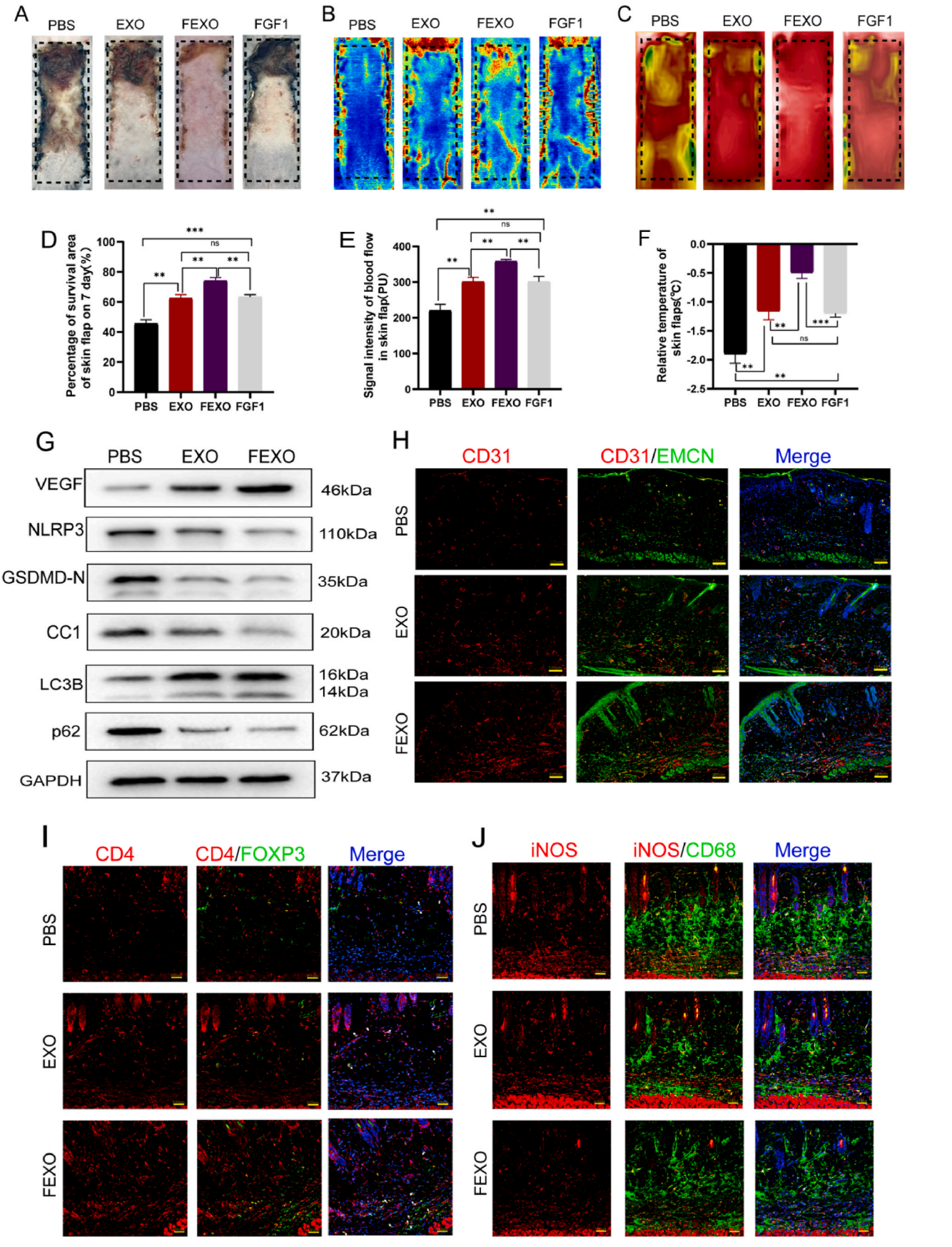

(caption on next page)

Fig. 2. FEXO promoted angiogenesis and autophagy, inhibited oxidative stress and alleviated apoptosis and pyroptosis in random-pattern skin flaps. (A) Digital image of RPSFs on D7 in PBS, EXO, FEXO and FGF1 groups. (B) The LDBF images of RPSFs in PBS, EXO, FEXO and FGF1 groups on D7. (C) Digital image of Infrared thermal imager of RPSFs in PBS, EXO, FEXO and FGF1 groups on D7. (D) The percentage of survival area in PBS, EXO, FEXO and FGF1 groups (n = 5). (E) The analysis of flood flow in each group (n = 5). (F) The relative temperature of RPSFs in each group (n = 5). (G) The WB for VEGF, NLRP3, GSDMD-N, Cleaved Caspase-1(CC1), LC3B and p62 expressions in the PBS, EXO and FEXO group. The gels have been run under the same experimental conditions, and cropped blots were used here. (H) The immunofluorescence images of CD31/EMCN positive vessels of skin flaps in PBS, EXO and FEXO groups. (I) The immunofluorescence images of CD4/Foxp3 Treg cells in PBS, EXO and FEXO group. (J) The immunofluorescence images of iNOS/CD68 M1 macrophages in PBS, EXO and FEXO group. * stands for $P < 0.05$, ** stands for $P < 0.01$, *** stands for $P < 0.001$, ns stands for not significant.

punctua in OGD-induced endothelial cells (Fig. 3 B, D). Western blot assay further confirmed that EXO and FEXO enhanced angiogenesis and autophagy and alleviated pyroptosis in OGD-induced endothelial cells (Fig. 3 E-F). Wound scratch assays (Fig. 3. G), Transwell (Fig. 3 H) and tube formation (Fig. 3 I) were used to assess the viability of OGD-induced endothelial cells. The results revealed that EXO and FEXO augmented the number of migrated cells and tubes (Fig. 3 K-L). It was also found that EXO and FEXO markedly enhanced the migration area of endothelial cells (Fig. 3. M). Flow cytometry analysis was also used to discover the effect of FEXO on macrophage polarization (Fig. 3. J). The FEXO inhibited the inflammation by reducing the percentage of M1-like macrophage (Fig. 3. N), and enhancing mRNA level of CD206 in macrophage (**SF 1. S**).

Furthermore, it was indicated that EXO and FEXO decreased TUNEL intensity in OGD-induced endothelial cells (**SF 1. J, P**). DHE staining and CYC IF intensity in the cells confirmed that EXO and FEXO also suppressed the level of oxidative stress (**SF 1. K, Q**) and apoptosis (**SF 1. L, R**). Taken together, these results revealed that FEXO enhanced autophagy and viability and alleviated pyroptosis and apoptosis in endothelial cells.

2.5. FEXO promoted angiogenesis and inhibited oxidative stress, pyroptosis and apoptosis in random-pattern skin flaps through autophagy

The GO pathway analysis of significant microRNAs downstream manifested that autophagy, oxidative stress, apoptosis and pyroptosis were involved in FEXO (Fig. 4. A). Notably, autophagy showed the moast significant function. To verify the GO analysis, several inhibitors and inducers were then administered to investigate the effects of different pathways on RPSFs treated with FEXO, including 3-MA (an autophagy inhibitor), Antcin A (a pyroptosis inducer), PETCM (an apoptosis inducer) and DMNQ (a ROS inducer). All drugs, especially for 3-MA, significantly impaired angiogenesis and survival rate of RPSFs **(SF. 3 A-D).** Therefore, autophagy might be the most significant pathway in FEXO rescuing skin flaps.

3-MA were administered with PBS, EXO or FEXO to further validate the role of autophagy in rescuing skin flaps. The survival area and blood flow of PBS group were decrease by inhibiting autophagy, and the FEXO significantly resist the pro-necrosis effects of 3 MA, followed by EXO (Fig. 4 B-C/F-G). IF image showed that 3-MA reduced the number of blood vessels in skin flaps. However, FEXO showed the best function on angiogenesis (Fig. 4 D, H). The western blot (Fig. 4. E) revealed that 3-MA impaired angiogenesis, autophagy and aggravated pyroptosis of skin flaps. The exosomes, especially for FEXO, significantly reversed the effects of 3-MA (**SF 3. O-T**). The Caspase-1 analysis in skin flaps indicated that FEXO reduced the activity of the enzymes induced by 3-MA (Fig. 4 I). Additionally, 3-MA aggravated oxidative (**SF 3. F, K**) and apoptotic injuries (**SF 3. H, M**) in EXO and FEXO group. Taken together, the findings confirmed the pro -survival effects of autophagy on skin flaps survival, and inhibiting autophagy would aggravate necrosis. FEXO showed the most superior effects in reduce the injuries of oxidation, apoptosis and pyroptosis through activating autophagy than EXO.

2.6. The application of 3 MA impaired the protective effects of FEXO on endothelial cells

IF images of GSDMD-N indicated that FEXO displayed better function in reducing the pyroptosis of endothelial cells induced by 3-MA (Fig. 5 A-B). Furthermore, it has been revealed that FEXO was more beneficial for restoring the autophagy flux than EXO (Fig. 5 C, G). The scratch wound (Fig. 5 D, H), transwell (Fig. 4 E, I) and tube formation assays (Fig. 4 F, J) demonstrated that FEXO significantly improved viability of OGD treated cells, followed by EXO. DHE (**SF 3. G, L**), TUNEL staining (**SF 3. E, J**) and CYC IF intensity (**SF3. I, N**) in endothelial cells confirmed that FEXO showed more contribution in reducing oxidative injury and apoptosis following autophagy blockage in contrast to EXO. These results further proved the important effects of autophagy in alleviating OGD endothelial cells injuries. And FEXO is more helpful in activating autophagy to protect cells.

2.7. Exosomal miR-183-5p derived from F-ADSCs improved angiogenesis and survival rates and alleviated pyroptosis in random-pattern skin flaps

Based on the transcriptome sequencing of microRNA of EXO and FEXO (Fig. 6 A-C), several significant up-regulated (miR-6990-5p and miR-183-5p) and down-regulated microRNAs (miR-5128, miR-3473e and miR-373b) were selected for validation. Different exosomes ($FEXO^{NC}$, $FEXO^{anti\text{-}miR-6990-5p}$, $FEXO^{anti\text{-}miR-183-5p}$, $FEXO^{miR-5128\text{-}mimic}$, $FEXO^{miR-3473e\text{-}mimic}$ and $FEXO^{miR-3473b\text{-}mimic}$) were extracted for further analysis of microRNAs functions in skin flaps. Exosomal miR-6990-5p showed less effects in skin flaps survival. And the skin flaps displayed severe necrosis after upregulating miR-5128, miR-3473e and miR-3472b in FEXO. The inhibition of exosomal miR-183-5p significantly aggravated necrosis **(SF 4. A-B)**. Moreover, the level of miR-183-5p was upegulated in necrotic area of mice skin flaps (**SF 4. R**). Therefore, miR-183-5p was selected as a potential target of FEXO due to the its significant influence on skin flaps. The expression level of miR-183-5p in ADSCs and exosomes was further confirmed using the qPCR technique (**SF 4. C-F**). The results revealed that the level of miR-183-5p was higher in the FEXO group than in the EXO group in random-pattern skin flaps and endothelial cells (**SF 4. G-J**). In addition, KEGG pathway classification revealed several pathways including the PI3K/AKT, mTOR and MAPK pathways (Fig. 6. D).

The elevated miR-183-5p in FEXO led us to verify whether miR-183-5p has a positive effect on autophagy in ischemic RPSFs. F-ADSCs were treated with miR-183-5p antigomirs or antagomir NC and extracted exosomes (FEXO, $FEXO^{NC}$ and $FEXO^{anti\text{-}miR-183-5p}$) to inject into the mice. It was observed that the levels of survival area and blood flow were significantly lower in the $FEXO^{anti\text{-}miR-183-5p}$ group than in the $FEXO^{NC}$ group and 3-MA co-administration further exacerbated the damage to RPSFs (Fig. 6 E-F/SF 4. K-L). Western blot assay demonstrated that the protein expression levels of VEGF were markedly downregulated in the skin flaps and the expression level of pyroptosis-associated proteins (NLRP3, GSDMD-N and CC1) were drastically upregulated in the $FEXO^{anti\text{-}miR-183-5p}$ group compared to the $FEXO^{NC}$ group (Fig. 6. G). $FEXO^{anti\text{-}miR-183-5p}$ blocked autophagy by reducing the level of LC3BII and elevating the level of p62 (Fig. 6. G/SF 5. L- Q). In addition, the application of 3-MA downregulated the expression of VEGF and aggravated pyroptosis in skin flaps. The depletion of exosomal miR-183-5p resulted in decreased CD31/EMCN positive blood vessels (Fig. 6. H/SF 4. M) and a subsequent increase in Caspase-1 activity in RPSFs (**SF 5. R**). Administration of $FEXO^{anti\text{-}miR-183-5p}$ also decrease the infiltration of Treg cells (Fig. 6. I/SF 4. N) and increase M1 macrophage in skin flaps (Fig. 6. J/SF 4.O). Furthermore, The results showed that the levels

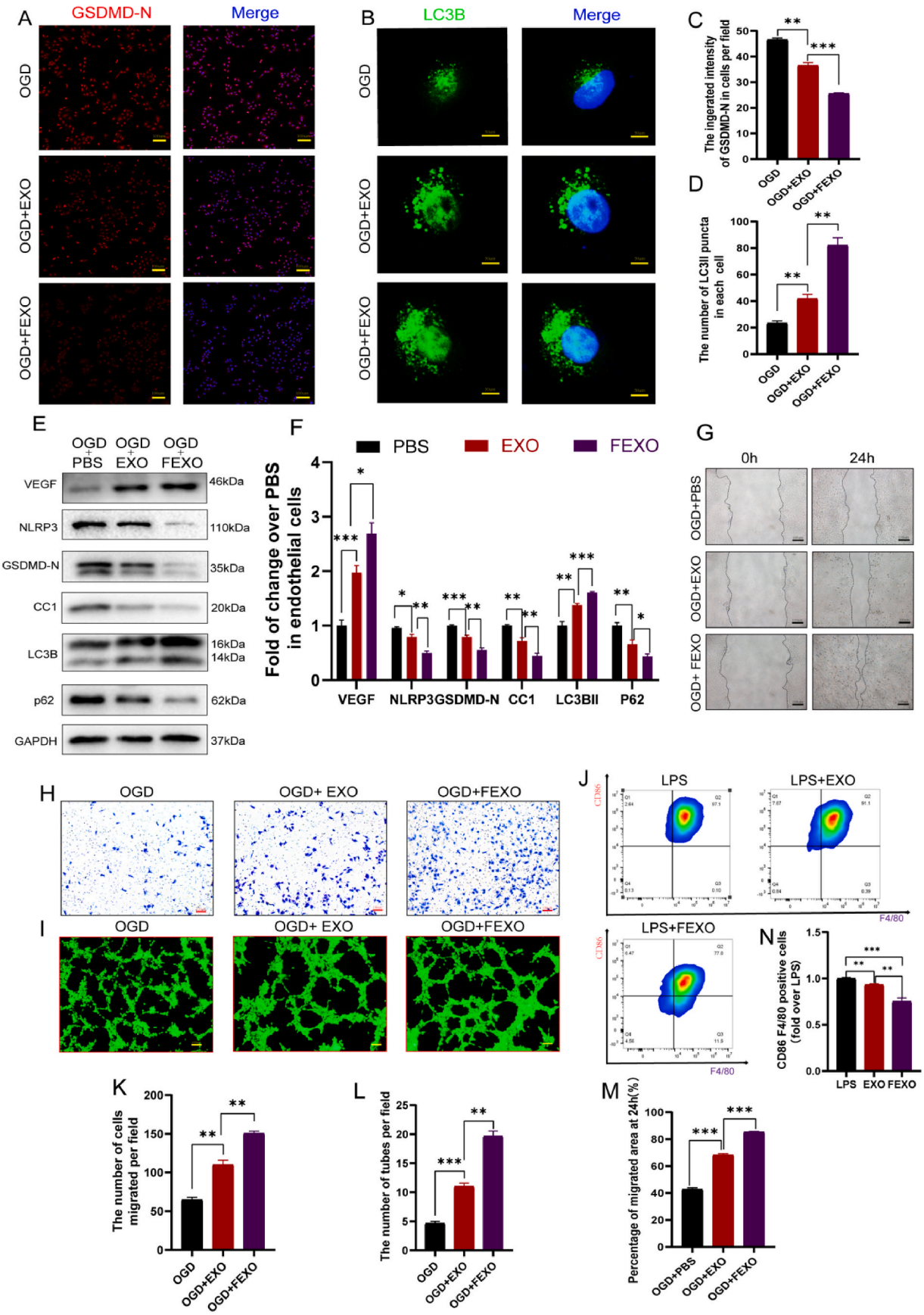

(caption on next page)

Fig. 3. FEXO enhanced autophagy and viability and alleviated pyroptosis in endothelial cells. (A) The immunofluorescence images of GSDMD-N in OGD endothelial cells. (B)The immunofluorescence images of LC3B puncta in OGD endothelial cells. (C) The analysis of immunofluorescence intensity of GSDMD-N in OGD endothelial cells (n = 3). (D) The number of activated LC3B punctua in each OGD endothelial cell was calculated (n = 3). (E) The WB of OGD endothelial cells (Bend3) treated with PBS, EXO and FEXO. The gels have been run under the same experimental conditions, and cropped blots were used here. (F) The density value of the proteins previously described in each group (n = 3). (G) The images of scratch wound assay are in OGD + PBS, OGD + EXO, and OGD + FEXO groups. (H) The images of transwell assay by endothelial cells in OGD + PBS, OGD + EXO and OGD + FEXO groups. (I) The image of tubes formed of endothelial cells in OGD + PBS, OGD + EXO and OGD + FEXO groups. (J) Flow cytometry image and quantification of M1-like macrophage. (K–L) The analysis of the tubes formation and migrated cells in each group (n = 3). (M) The percentage of migrated area by scratch wound assay was analyzed in each group (n = 3). (N) the analysis of M1-like mecrophage. * stands for $P < 0.05$, ** stands for $P < 0.01$, *** stands for $P < 0.001$, ns stands for not significant.

of oxidative stress (**SF 5. B, G**) and apoptosis (**SF 5. D, I**) in skin flaps were also elevated by FEXO$^{anti\text{-}miR-183-5p}$. Therefore, the above findings suggested that exosomal miR-183-5p derived from F-ADSCs improved angiogenesis and survival and alleviated pyroptosis and apoptosis in random-pattern skin flaps.

2.8. Endothelial cells with exosomal miR-183-5p inhibited autophagy, viability and pyroptosis

The inhibitory effects of exosomal miR-183-5p on autophagy in endothelial cells were analyzed. The results showed that FEXO inhibited the exosomal miR-183-5p from increasing the intensity of GSDMD-N in endothelial cells (Fig. 7 A-B). Furthermore, the number of LC3B punctua was decreased by FEXO$^{anti\text{-}miR-183-5p}$ (Fig. 7 C-D). The scratch wound (Fig. 7 E-F), transwell (Fig. 7 G-H) and tube formation assays (Fig. 7 I-J) indicated that FEXO$^{anti\text{-}miR-183-5p}$ decreased the viability of endothelial cells. In addition, it was discovered that miR-183-5p in FEXO could inhibit the inflammatary phenotype of macrophage by reducing percentage of M1 cells, and increase the CD206 mRNA of M2-like mcrophag (Fig. 7 K-L/SF 5. K). TUNEL (**SF 4. A, F**) staining showed that depletion of miR-183-5p in FEXO aggregated the rupture of DNA strands in endothelial cells. The staining using DHE (**SF 4. C, H**) and the fluorescence caused by CYC (**SF 4. E, J**) were also examined to validate the effects of exosomal miR-183-5p on HUVEC. Therefore, the results showed that FEXO$^{anti\text{-}miR-183-5p}$ significantly augmented the level of ROS and apoptosis in different cells.

In order to further investigate the side effects of miR-183-5p, the microRNA mimics were directly transfected into HUVEC, L929 and Hacat cells. CCK8 analysis proved that the viability of uninjured cells wasn't influenced by miR-183-5p. Moreover, the miR-183-5p significantly alleviate injuries of above cells after OGD treatment **(SF 2. F-H)**. In addition, miR-183-5p was proved the same function in inhibiting the oxidation and apoptosis of L929 and Hacat cells as in HUVECs **(SF 5. S-Z)**. Overall, miR-183-5p showed significant therapeutic effects in cutaneous cells.

2.9. Exosomal miR-183-5p regulated autophagy by targeting GPR137 through PI3K/AKT/mTOR signaling axis

It was reported that G protein-coupled receptors (GPRs) play important roles in ischemic disease [33]. Based on the transcriptome sequencing analysis of patients skin flaps, several GPRs were downregulated in necrotic area **(SF 6. A)**. PCR results indicated that GPR137 was the most significantly downregulated mRNA in mice skin flaps **(SF 6. B)**. Meanwhile, GPR137 has been predicted as a target of elevated miR-183-5p in necrotic mice skin flaps. Therefore, the effects of exosomal miR-183-5p/GPR137 on RPSFs and endothelial cells were verified.

Wild-type and mutant sequences of GPR137's 3′-UTRs were analyzed. It has been demonstrated that the overexpression of miR-183-5p significantly reduces the activity of the luciferase enzyme in wild-type mice. The mutated group did not exhibit any inhibitory effects on luciferase activity (Fig. 8 A-B). To validate the impact of miR-183-5p/GPR137 on autophagy, GPR137 was overexpressed in endothelial cells. Mechanistically, the results showed that GPR137 augmented the expression of NLRP3, p62, P-PI3K/PI3K, P-AKT/AKT and P-mTOR/mTOR and suppressed the expression of VEGF and LC3BII in endothelial cells (Fig. 8. C/SF 8. D-J). IF staining indicated that GPR137 upregulated the expression of GSDMD-N (Fig. 8. D/SF 7. Q) and decreased the number of LC3B puncta in endothelial cells (Fig. 8. E/SF 7. R). Transwell (Fig. 8. G/SF 7. S), tube formation (Fig. 8. H/SF 7. T) and wound scratch assays (Fig. 8. I/SF 7. U) showed that GPR137 markedly reduced viability in endothelial cells. What' s more, overexpression of GPR137 could also accelerate the progress of inflammation by modulating the polarization of macrophage (Fig. 8. F/SF 5. V). The results of DHE (**SF 7. A, F**), TUNEL (**SF 7. B, G**) staining and CYC immunofluorescence **(SF 7. C, H)** assays provided evidence that GPR137 reduced the protective effects of FEXO on oxidative stress and apoptosis. Taken together, these results concluded that exosomal miR-183-5p regulated autophagy by targeting GPR137 through the PI3K/AKT/mTOR signaling pathway.

2.10. FEXO might possess a better efficiency and clinical superiority in ischemic random -pattern skin flaps

Although FGF1 and EXO are proven drugs in cutaneous regeneration, long-term and multiple administration are usually required in clinical application. The great efficacy and mechanism of FEXO rescuing RPSFs were confirmed. In the following study, further investigation was launched to determine the clinical efficiency of FGF1, EXO and FEXO (Fig. 8. J). Surprisingly, a single dose of FEXO in the middle of surgery significantly inhibit the necrosis of the mice RPSFs. While, extra administration of FGF1 (extra 2 times) or EXO (extra 1 time) after surgery are still needed to reach the same effectiveness as FEXO. In addition, direct drops of FEXO to the wound before RPSFs sutures also accelerate the recovery of skin flaps (Fig. 8 K-N).

Invasive operation after the skin flaps surgery should be maximum inhibited, for extra injections would bring severe risks of pain sensation, skin flap necrosis and infections. The application of FEXO not only reduces the frequency of administration, but also decreases the additional damage caused by post-surgery subcutaneous injections. Therefore, the engineering FEXO is more effective and superior than existing clinical treatments (FGF1 or EXO) in skin flaps regeneration.

2.11. GPR137 might also be a new therapeutic target for random-pattern skin flaps

It is notable that the levels of GPR137, P-PI3K/PI3K, P-AKT/AKT and P-mTOR/mTOR were downregulated in the PBS group compared to the Sham group (no surgery group), while the expression level of LC3BII was augmented in the PBS group (Fig. 9 A, H-L). EXO, FEXO$^{anti\text{-}miR-183-5p}$ and FEXO obstructed the activation of GPR137 and Pi3K/Akt/mTOR pathway (Fig. 9 A, H-L). Based on the results above, it was hypothesized that GPR137 might serve as a new target for RPSFs. Further experiments revealed that overexpressed GPR137 abolished the protective effects of exosomal miR-183-5p of FEXO on RPSFs with the highest survival rate and blood flow (Fig. 9 B-E). The phosphorylation of Pi3k/Akt/mTOR pathway were also influenced by upregulation and downregulation of GPR137 **(SF 6. C/E-H)**. The expression of GPR137 also decreased the number of CD31/EMCN-positive blood vessels (Fig. 9 F-G). DHE staining and CYC immunofluorescence intensity confirmed that GPR137 aggregated oxidative injury and apoptosis in skin flaps (**SF 7. D-E, I-J**). Therefore, the above findings suggested that GPR137 might be a new therapeutic target for random-pattern skin flaps.

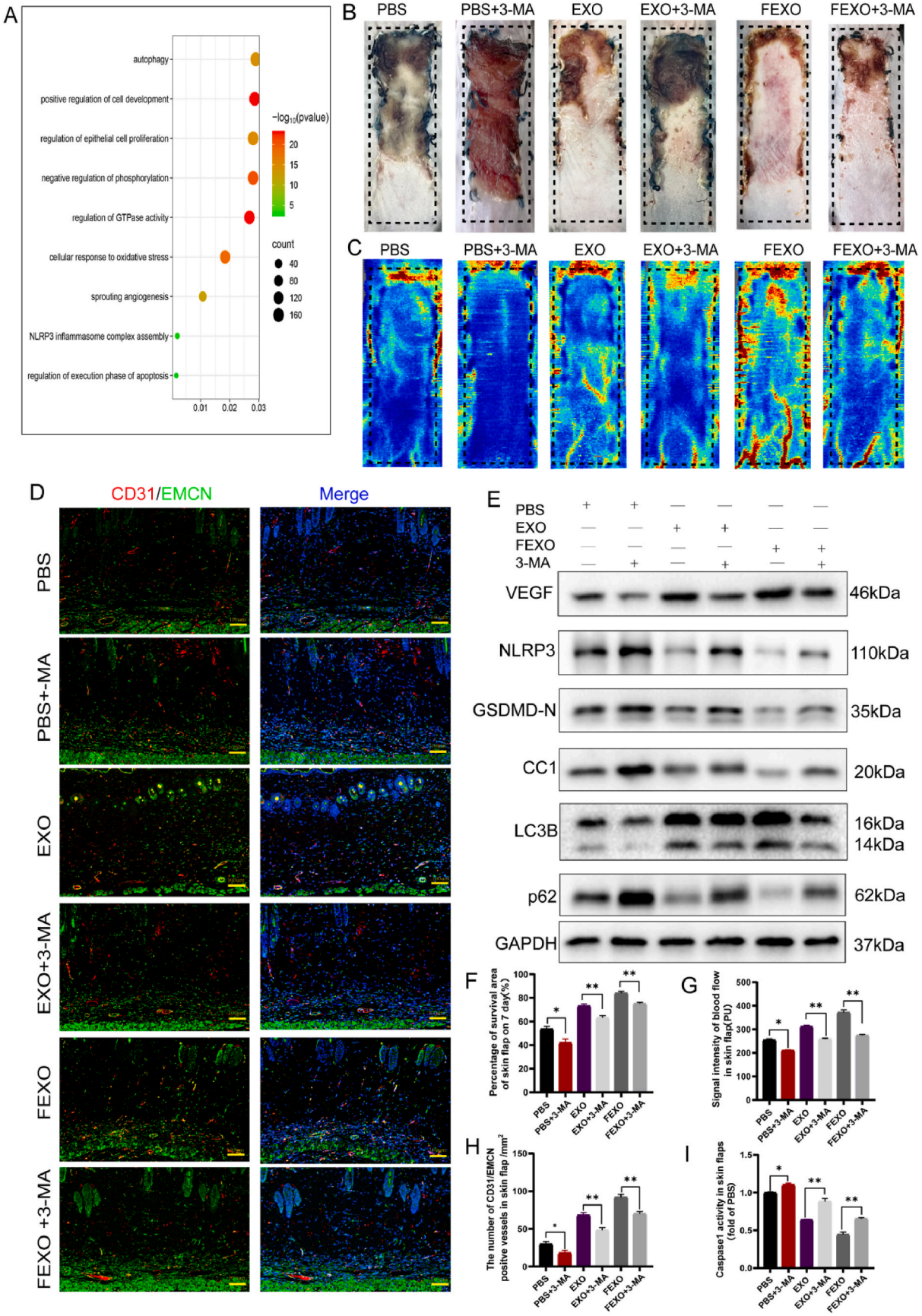

(caption on next page)

Fig. 4. FEXO promoted angiogenesis and inhibited oxidative stress, pyroptosis and apoptosis in random-pattern skin flaps through autophagy. (A) The GO pathway analysis of significant microRNA downstream in FEXO and EXO. (B) Digital image of RPSFs on D7 in PBS, PBS + 3-MA, EXO, EXO + 3-MA, FEXO and FEXO + 3-MA groups. (C)The full field LDBF images of RPSFs in PBS, PBS + 3-MA, EXO, EXO + 3-MA, FEXO and FEXO + 3-MA groups on D7. (D) The immunofluorescence images of CD31/EMCN positive vessels of skin flaps in PBS, PBS + 3-MA, EXO, EXO + 3-MA, FEXO and FEXO + 3-MA groups. (E) The expression of angiogenesis-related protein VEGF; pyroptosis-related proteins NLRP3, GSDMD-N and Cleaved Caspase-1(CC1) and autophagy-related proteins LC3B, and p62 in PBS, PBS + 3-MA, EXO, EXO+3-MA, FEXO and FEXO + 3-MA groups. The gels have been run under the same experimental conditions, and cropped blots were used here. (F) The percentage of survival area in each group (n = 5). (G) The signal intensity of blood flow of flaps was analyzed in each group (n = 5). (H) The number of CD31/EMCN positive vessels were analyzed in each group (n = 3). (I) The activity of Caspase-1 in skin flaps (n = 3). * stands for $P < 0.05$, ** stands for $P < 0.01$, *** stands for $P < 0.001$, ns stands for not significant.

2.12. FEXO promoted the healing rate of mice chronic diabetic wounds

Skin flaps surgery are convenient strategies for wound regeneration in clinics, but the operation would still bring unpredictable risks. Therefore, the effects of FEXO on chronic diabetes wounds were also discovered. The solution of FGF1, EXO and FEXO were carefully dropped on wounds at the concentration previously mentioned (50ul for each wound). Surprisingly, the FEXO significantly improved the recovery of mice chronic wound (**SF 8. A-C**). FEXO showed less time in wound closure than EXO or FGF1. In conclusion, FEXO might be a promising treatment in cutaneous regeneration according to RPSFs and diabetes wound models.

3. Discussion

Skin flaps surgery are commonly applied in clinics to reconstruct cutaneous defects, especially for RPSFs. However, the ratio of length to width of RPSFs should generally not exceed 2:1, which restricts their usage in clinical settings. RPSFs are not suitable for reconstructing massive and complex skin defects because of the possible necrosis of skin flaps. Perforator skin flaps, free skin flaps and axial flaps, were also used in clinic as previously mentioned, but the procedures are more complicated, and always cause severer damage to elderly patients than RPSFs. Pressure injuries always result in skin wound in clinics. Long-term ischemia or repeated ischemia-reperfusion have been confirmed a severe damage to surrounding cutaneous microcirculation [34] , which might further lead to the insufficient blood supply and ischemia of reconstructive RPSFs. 6 patients who suffered from pressure ulcers and underwent reconstructive surgery of RPSFs were recruited in our clinic trail to determine the therapeutic targets. This study mainly focused on RPSFs and aim to establish a new strategy to solve the ischemic skin flaps.

In this study, FGF1 (mRNA and protein level) were significantly elevated in necrotic area of RPSFs both in patients and mice on the seventh day following surgery. FGF1 may represent a protective growth factor against ischemia in skin flaps. FGF1 enhanced the survival rate of the mice skin flaps to some extent at the concentration of 15ug/ml, but the distal portion of the flaps still showed evidence of partial necrosis (**SF 1. C-D**). FGF1 would bring potential aberrant proliferative and carcinogenic risks in clinics. Lee et al. suggest that the natural structures of FGF1 make it more susceptible to proteases and unstable in complex internal environments, which results in short half-lives of endogenous and exogenous FGF1 *in vivo* [35]. Studies have revealed that ischemic skin flaps are caused by the rupture of the lysosomal membrane [36]. The leakage of proteases from lysosomes would result in the breakdown of FGF1. In addition, researchers have revealed that FGF1 possesses immunogenic potential due to the presence of buried free cysteine residues (Cys) [37]. The limitation of FGF1 might be due to its structure and short half-life in harsh microenvironments and a new strategy is urgently required to preserve RPSFs and solve the insufficiency of FGF1.

Emerging evidence suggests that exosomes maintain their stability and rigidity due to their excellent lipophilic properties [38,39]. A recent study indicates that the phospholipid bilayer of exosomes significantly protects their contents from degradation [40]. It has been confirmed that exosomes have high efficiency and low immunogenicity, which makes them a potential clinical strategy [41,42]. It was confirmed that the EXO partially improved the survival rate of RPSFs at 100ug/ml, while higher concentration of EXO might display severe side effects of necrosis (**SF 1. A-B**). Unique characteristics of exosomes may prevent FGF1 from degradation, and the combination of FGF1 with exosomes also reduced the side effects of EXO. Therefore, FGF1-preconditioned ADSCs exosomes (FEXO) were applied to RPSFs and discovered that the efficacy was better than EXO or FGF1.

Aberrant angiogenesis, programmed cell death including pyroptosis apoptosis and oxidative stress induces skin flap ischemia [43,44]. Growing evidence indicates that VEGF plays an important role in angiogenesis and tissue regeneration [45,46]. In this study, it was observed that FEXO augmented the expression levels of VEGF in both endothelial and skin flap cells. Researchers discovered that the survival rate of skin flaps could be significantly improved by increasing temperature, and higher temperature reflects better prognosis of the skin flaps [47,48]. In addition, the blood flow of skin flaps could be converted into thermal image by temperature prediction devices [49]. Therefore, higher temperature tend to represent skin flaps vascular reconstruction and survival. The increased temperature indicated that FEXO significantly improved the viability of skin flaps. Laser Doppler instruments are also widely applied to detect flood flow image in skin flaps [50]. Enhanced temperature and blood flow of skin flaps were discovered in FEXO group, implying that FEXO improved the angiogenesis and survival rate of RPSFs. Pioneering research showed that EMCN and CD31 are markers located on the endothelial cells that estimate newborn vascular development [51]. Therefore, the blood flow signal intensity, temperature and number of CD31/EMCN-positive blood vessels in the skin flap were analyzed. It turned out that FEXO demonstrated the most potent effects on angiogenesis.

Pyroptosis is a recently uncovered form of programmed cell death caused by activating GSDMD-N protein translocating to the membrane, resulting in membrane rupture and death [52,53]. The FEXO significantly alleviated pyroptosis by downregulating the expression of NLRP3, GSDMD-N and CC1. Accumulating evidence proves that ischemia results in the activation of oxidative stress and apoptosis [54,55]. FEXO inhibited oxidative stress and alleviated apoptosis and by reducing the accumulation of ROS and CYC in skin flaps and OGD-induced endothelial cells.

Autophagic progress is the combination of autophagosomes and lysosomes to eliminate and recycle intracellular compounds [56]. Autophagy usually determines the outcome of a variety of diseases [57]. In addition, the exosomes induced autophagy would ameliorate vascular diseases [58]. The results indicated that FEXO suppressed apoptosis and pyroptosis and elevated autophagy flux in skin flaps and endothelial cells. To further understand the most influential factor, the skin flaps were separately injected with 3-MA [59], DMNQ [60], Antcin A [61] and PETCM [62] for 7 days. The survival of skin flaps was mostly determined by FEXO-associated autophagy followed by pyroptosis, apoptosis and oxidative stress. Based on these results, autophagy might be the most significant pathway in the treatment of ischemic skin flaps by FEXO. In this research, 3-MA was administered to examine the interaction between autophagy, pyroptosis and apoptosis. Intriguingly, 3-MA aggregated apoptosis, pyroptosis and oxidative stress of RPSFs. The results indicated that FEXO was primarily associated with the induction of autophagy in RPSFs.

MicroRNAs (miRNAs) are small non-coding RNAs that regulate gene

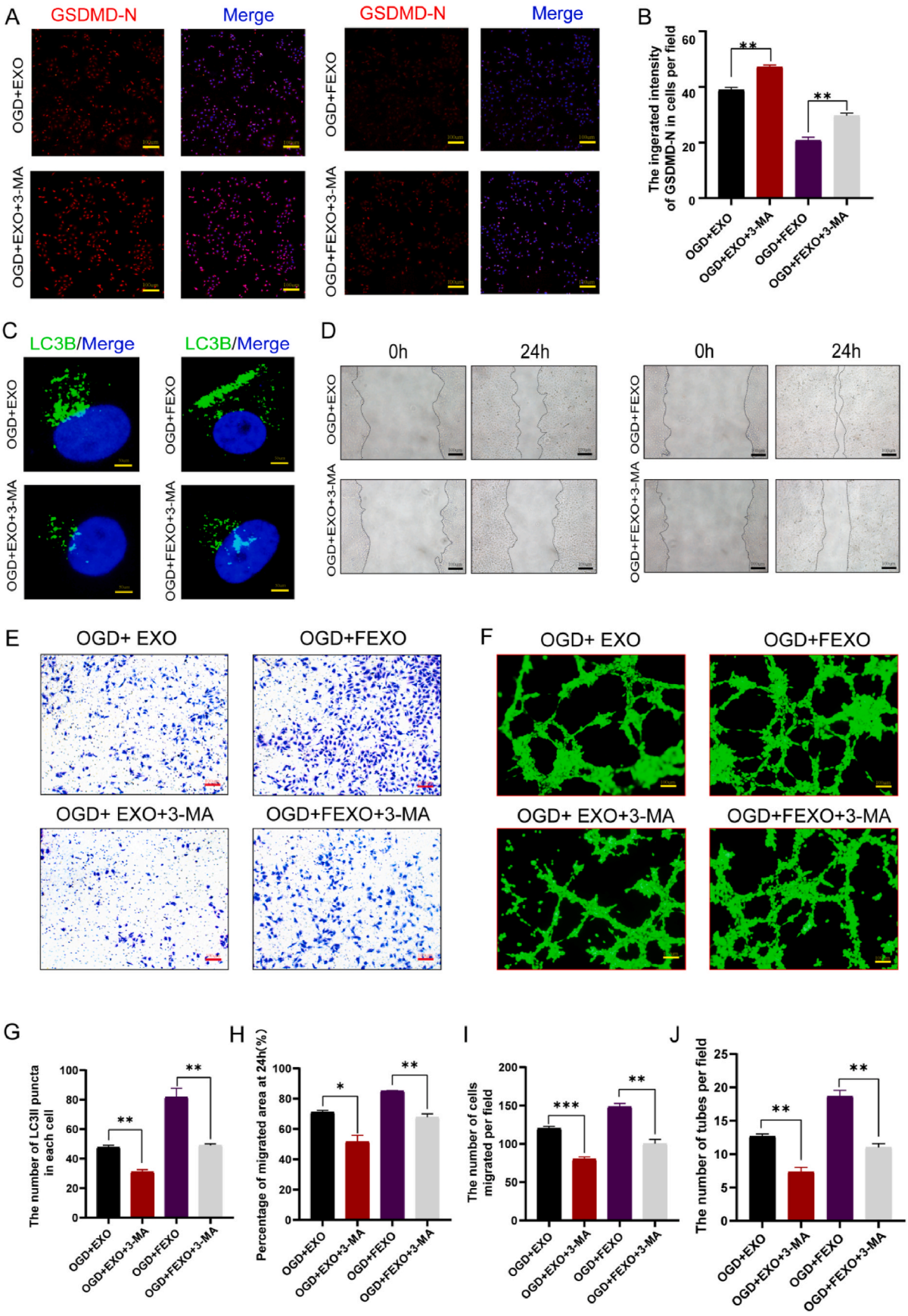

(caption on next page)

Fig. 5. The application of 3 MA impaired the protective effects of FEXO on endothelial cells. (A)The immunofluorescence images of GSDMD-N in endothelial cells. (B)The immunofluorescence intensity of GSDMD-N was analyzed in each group (n = 3). (C) The immunofluorescence images of LC3B puncta in OGD endothelial cells. (D)The image of scratch wound assays in EXO, EXO + 3-MA, FEXO and FEXO + 3-MA groups. (E)The image of the transwell assay in EXO, EXO + 3-MA, FEXO and FEXO + 3-MA groups. (F) The image of tube formations in EXO, EXO + 3-MA, FEXO and FEXO + 3-MA groups. (G) The number of activated LC3B puncta in each OGD endothelial cell was calculated (n = 3). (H) The percentage of migrated area by scratch wound assay was analyzed in each group (n = 3). (I) The number of migrated cells in each group from transwell assays (n = 3). (J) The number of tubes in each group (n = 3).* stands for $P < 0.05$, ** stands for $P < 0.01$, *** stands for $P < 0.001$, ns stands for not significant.

expression post-transcriptionally [63,64]. To clarify the potential mechanism, the microRNA levels were examined in FEXO. It was clear that miR-6990-5p, miR-183-5p were up-regulated and miR-5128, miR-3473b and miR-3473e were down-regulated in FEXO. The inhibition of miR-6990-5p displayed less influences on skin flaps survival, implying that miR-6990-5p might not be a target of FEXO. Study has pointed out that miR-5128 and miR-3473e possess the pro-inflammatory effects through stimulating M1 macrophage polarization, and miR-3473b has been proved a target in aggravating ischemia [65,66], which might explain the overexpression of exosomal miR-5128, miR-3473e and miR-3473b in FEXO resulted in severe necrosis of skin flaps. However, inhibition of exosomsal miR-183-5p aggravated RPSFs necrosis, indicating that miR-183-5p might played an important role in skin flaps survival.

Previous studies have confirmed the function of microRNAs in autophagy regulation [67,68]. In addition, miR-183-5p inhibits the activation of autophagy by suppressing the expression of Becline and Atg5 [69,70]. According to our results, miR-183-5p in FEXO probably regulated autophagy positively. Knockdown of miR-183-5p blocked the activation of autophagy in exosomes. In addition, $FEXO^{anti\text{-}miR-183-5p}$ reduced the survival rate and blood flow level of RPSFs. It was verified that autophagy flux mediated by miR-183-5p protected FEXO from pyroptosis, apoptosis and oxidative stress.

G protein-coupled receptors (GPRs) are transmembrane proteins that regulate a variety of biological processes such as the phosphorylation of proteins and the development of tumors [71]. GPR137 was proved to be a direct targets through luciferase assays. Studies have revealed that GPR137 promotes cell proliferation and differentiation [72–74]. However, the regulation of GPR137 on autophagy remains elusive. The overexpression of GPR137 inhibited viability and reduced the protection of exosomal miR-183-5p from apoptosis, pyroptosis and oxidative stress in OGD endothelial cells. In addition, the results suggested that GPR137 is a negative regulator of autophagy, as the expression of GPR137 inhibited LC3B in endothelial cells.

RPSFs showed a decrease in GPR137 on the 7th day post-surgery compared to the sham group (no surgery). Whether GPR137 may also have the potential for skin regeneration need to be further validated. The downregulation of GPR137 increased angiogenesis and survival rates of skin flaps, thereby suggesting that GPR137 could be a new therapeutic target for RPSFs. The present study mainly focused on elucidating the downstream signaling pathway of GPR137 on autophagy. PI3K/AKT/mTOR are intracellular signaling pathways implicated in metabolism, proliferation, cell survival and growth [75]. Researchers revealed that the phosphorylation of mTOR disrupts autophagy flux [76]. Mechanistically, the exosomal miR-183-5p obstructed the activation of the PI3K/AKT/mTOR signaling axis, whereas the overexpression of GPR137 increased the phosphorylation levels of the pathway. MiR-183-5p/GPR137 was shown to induce autophagy-related protection in skin flaps by modulating the PI3K/AKT/mTOR signaling pathways.

It was reported that immune cells regulate the injuries of inflammation [77]. The inhibition of M1-like macrophage would reduce the damage in ischemic disease [78]. Treg cells possess the anti-inflammatory and cutaneous regenerative fuction [79,80]. Pi3k/Akt pathway were also involved in the M1 polaraization and Treg cells development [81,82]. The inhibition of Pi3k/Akt pathway may result in reduced polarization of M1 macrophage and activated Tregs function, which further explain FEXO associted miR-183-5p/GPR137/Pi3k/Akt pathway in macrophage and Treg cells infiltration. In addition, the Treg cells secrete TGF-β to inhibit M1 polarization [83]. Taken together, FEXO is involved in immune regulation and reduced the inflammatory response in cutaneous ischemic disease.

Despite their prospective clinical value, exosomes production have limited translational potential [84]. The exosomes secretion is the process of vesicle membrane transportation and fusion [85], and increased rate of membrane fusion events would promote exosomes generation [86]. GO pathway indicated that the vesicle-related membrane fusion and transport were upregulated in FEXO, implying that FGF1 stimulated exosomes release. WB and NTA analysis of exosomes further proved that the exosmes secretion in ADSCs were enhanced by FGF1. It was reported that VAMPs proteins function in extracellular vesicle (EVs) transporting and membrane trafficking of cells [87]. Especially for VAMP3, the protein is located on the membrane and plays a pivotal role in the transportation and fusion of vesicles [32]. The present results indicated that the expression of VAMP3 in ADSCs influence the extracellular vesicle release. Taken together, FGF1 -stimulated exosomes secretion was mediated by VAMP3, which may provide new ideas for enhancing the engineering exosomes production.

Dosage administered usually determine the therapeutic effects. Multiple injections would increase the injection-related risks, such as pain sansation, infections (skin contaminants infiltrate the injection site at the time of injection) and so on [88,89]. Engineering FEXO not only solves the therapeutic restriction of FGF1 and EXO, but also shorten the frequency of administration in rescuing the RPSFs. Diabetic wounds were charactered with activated ROS and sustained inflammation [90]. This study has already confirmed the ability of FEXO in alleviating oxidative stress and inflammation. Therefore, engineering FEXO was applied for mice chronic diabetic wound, and was proved great effects than EXO and FGF1. Previous study have confirmed the effectiveness of FGF1 in cerebral and myocardial ischemia [91,92]. Based on the prominent effects of FEXO on cutaneous ischemic skin flaps, FEXO is an optional medication for cerebral and myocardial ischemic disease, which might improve the therapeutic effects of FGF1.

The superior short-term effects of FEXO on ischemic skin flaps was validated in present experiments. Study has reported a sustained-release exosomes in hydrogel for wound closure [93], indicating that exosomes displayed significant long-term therapeutic effects in chronic cutaneous disease. Therefore, FEXO would show good long-term effects through these sustained-release strategy in cutaneous ischemic diseases. In addition, the safety of exosomes has been demonstrated in relation to the heart, brain and kidneys [94]. Therefore, FEXO might show safety in cutaneous regeneration.

3.1. Clinical value, prospect and limitation of the study

The experiment has confirmed the therapeutic effects of FEXO on RPSFs and chronic diabetes wound. FEXO could be a selective strategy in clinic in cutaneous regeneration for the great effects in contrast to clinical proven drugs (EXO and FGF). FEXO could be administrated alone or acted as an selective component in manufacture of regenerative materials. In addition, FGF1 could enhanced the number of exosomes, which provide a valuable evidence for clinical translation of exosomes. The condition of skin flaps ischemia firstly occurs after surgery, and accompanied with delayed necrosis [95]. Surprisingly, the serum FGF1 level of the patients with skin flaps necrosis was significantly elevated in D3 after surgery, and GPR137 was also downregulated in ischemic skin

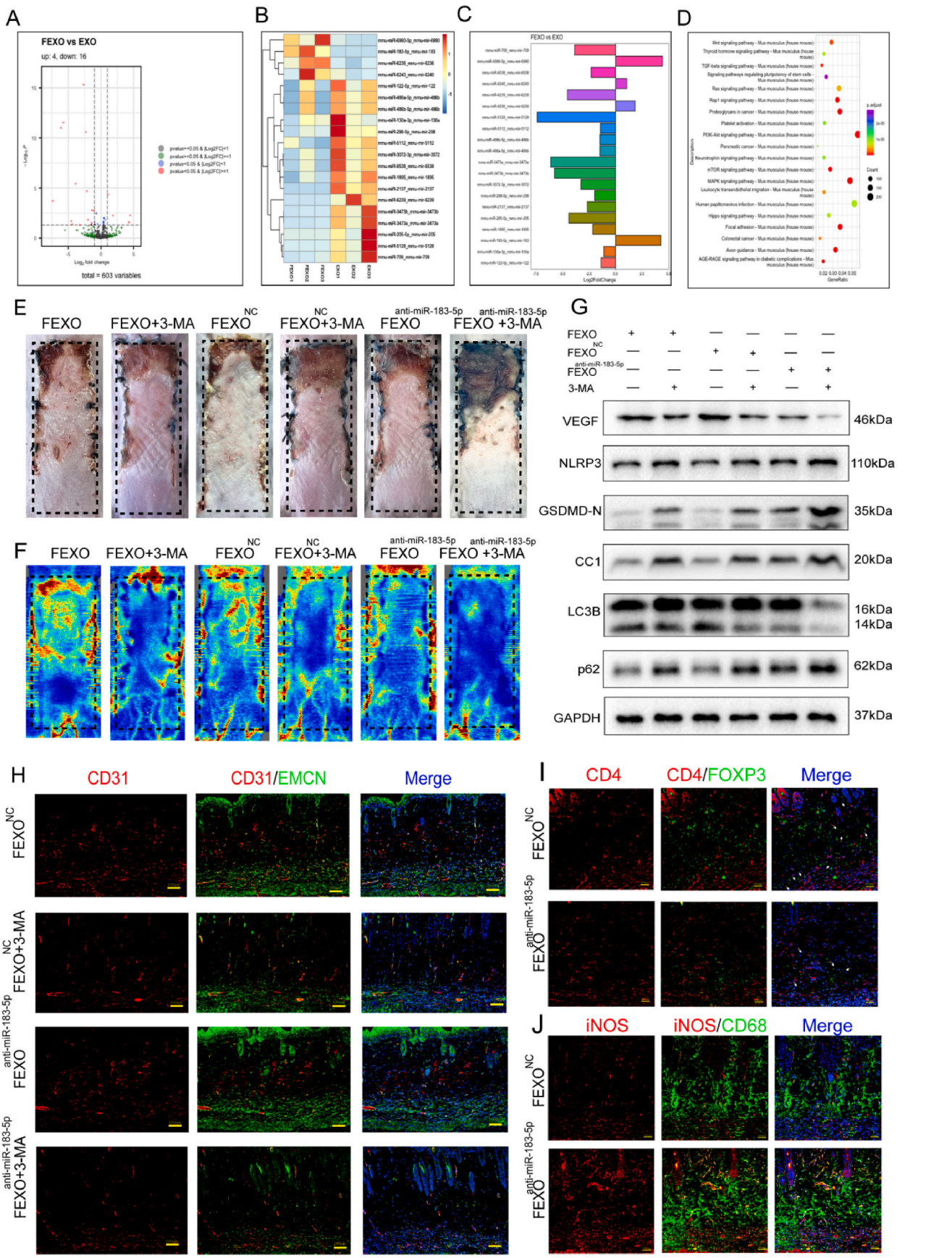

(caption on next page)

Fig. 6. Exosomal miR-183-5p derived from F-ADSCs improved angiogenesis and survival rates and alleviated pyroptosis in random-pattern skin flaps. (A) The volcano plot of miRNA expression difference in EXO and FEXO.(B–C) MicroRNAs expression profile showing the expression difference in EXO and FEXO (D) Representative signaling pathways of genes targeted by significantly differential miRNAs according to KEGG analysis. (E) Digital image of RPSFs on D7 in FEXO, FEXO + 3-MA, $FEXO^{NC}$, $FEXO^{NC}$ + 3-MA, $FEXO^{anti\text{-}miR-185-5p}$, $FEXO^{anti\text{-}miR-185-5p}$ + 3-MA. (F) The LDBF images of random -pattern skin flaps in FEXO, FEXO + 3-MA, $FEXO^{NC}$, $FEXO^{NC}$ + 3-MA, $FEXO^{anti\text{-}miR-185-5p}$, $FEXO^{anti\text{-}miR-185-5p}$ + 3-MA groups on D7. (G) The expression of angiogenesis-related protein VEGF; pyroptosis-related proteins NLRP3, GSDMD-N and Cleaved Caspase-1(CC1) and autophagy-related proteins LC3B and p62 in FEXO, FEXO + 3-MA, $FEXO^{NC}$, $FEXO^{NC}$ + 3-MA, $FEXO^{anti\text{-}miR-185-5p}$, $FEXO^{anti\text{-}miR-185-5p}$ + 3-MA groups. The gels have been run under the same experimental conditions, and cropped blots were used here. (H) The immunofluorescence images of CD31/EMCN positive vessels of skin flaps in $FEXO^{NC}$, $FEXO^{NC}$ + 3-MA, $FEXO^{anti\text{-}miR-185-5p}$, $FEXO^{anti\text{-}miR-185-5p}$ + 3-MA groups. (I) The immunofluorescence images of CD4/Foxp3 Treg cells in skin flaps. (J) The immunofluorescence images of iNOS/CD68 M1 macrophages in skin flaps. * stands for $P < 0.05$, ** stands for $P < 0.01$, *** stands for $P < 0.001$, ns stands for not significant.

flaps of patients and mice, indicating that FGF1 and GPR137 could be a prediction of possible ischemia.

Several studies touched on exosome therapy for skin flaps were presented in Supplementary Table 2 [96–100]. Study indicated ADSCs -EXO demonstrated more significant effects on angiogenesis than BMSC-EVs in cutaneous regeneration [101]. In addition, the acquisition of subcutaneous adipose stem cells is more convenient in clinics. Therefore, ADSCs were selected as the derivation of FEXO. Although hypoxia and H_2O_2 improved the effects of exosomes, study indicated that the oxidative substances and advanced glycation end-products (AGEs) were encapsulated in exosomes [102,103], which will bring extra damage to the recipient cells. Therefore, FGF1 was elected to be the modification strategy, due to the anti-oxidative and angiogenesis function in ischemic disease.

Although FEXO has displayed great effects on mice skin flaps, limitations of the experiments cannot be neglected. FEXO is under the experimental stage, and clinical translation might face numerous challenges. Further experiments will be concentrated on production processes, dose optimization, administration routes, and stability of FEXO. In addition, animal models that are more physiologically similar to humans, such as pigs or primates, will be also taken into consideration. Finally, a series of monitoring index and evaluation criteria were required to verify the effects during clinical translation.

4. Conclusion

In this research, It was found that FEXO made up for the deficiency of EXO and FGF1 on ischemic RPSFs. Engineering FEXO improved the survival rate of RPSFs by enhancing angiogenesis and autophagy and inhibiting pyroptosis, apoptosis and oxidative stress, which could be a new solution to improve the limitation of RPSFs in clinics. In addition, FGF1 promotes exosomes production by upregulating VAMP3, which may be a promising strategy for clinical application and translation in the future. Furthermore, the overexpression of GPR137 affects cell viability, pyroptosis and the survival of RPSFs, implying that GPR137 might be a new molecular target for rescuing ischemic skin flaps.

5. Materials and methods

5.1. Patients with skin flaps surgery

In order to maintain the accuracy and consistency of the experiment. Patients with cancer, diabetes or vascular morbidity which could affects cutaneous regeneration were excluded. Finally, 6 male patients were recruited in this experiments (3 patients were discovered with necrosis on the distal end of RPSFs, and others showed complete survive of skin flaps). The characters of patients were mentioned in Table 1 from supplementary data. The samples of 6 male patients who underwent RPSFs surgery because of sacrococcygeal pressure ulcers were obtained from Department of Wound healing, The First Affiliated Hospital of Wenzhou Medical University. The study was conducted in strict accordance with the ethical standards laid out in the Declaration of Helsinki II. Approval was granted by the Research Ethics Committee of the First Affiliated Hospital of Wenzhou Medical University (Protocol No. KY2023-294). Prior to participation, written informed consent was secured from all participants or their legal guardians, ensuring that they were fully informed of the study's scope and nature as well as any potential risks involved. The transcriptome sequencing analysis was used to detect the difference of mRNAs from 3 patients with necrosis on the distal end of RPSFs. The Elisa assays (Beyotime, PF319) were also applied for examining the serum concentration of FGF1.

5.2. Experimental animals

The mice were kept under standard conditions (temperature: 21–25 °C, humidity: 50–60 %, 12 h of light/dark cycle) with free access to food and water. The animals were handled with the approval of the Animal Committee at Wenzhou Medical University (XMSSQ2023-0005). The mice were obtained from the Experimental Animal Center of Wenzhou Medical University (license no. SCXK [ZJ] 2015-0001). The random-pattern skin flap (RPSF) model was established on the dorsum of C57BL/6 mice (male, 6–8 weeks old, average weight 25–30 g). The mice were anesthetized with 50 mg/kg of pentobarbital sodium injected intraperitoneally. The dorsal fur was then removed with an electric shaver and depilatory lotion. As previously described, a 1.5 by 4.5 cm caudally-based RPSF was applied in the mouse dorsum to remove the visible vessels beneath the skin flaps [12]. Experimental groups were allocated into the following groups: Sham (non-surgery), PBS (control), Scramble (Polyplus-transfection control), FGF1, EXO, FEXO, PBS+3-MA, EXO+3-MA, FEXO+3-MA, FEXO+3-MA, $FEXO^{anti\text{-}mir-183-5p}$, $FEXO^{anti\text{-}miR-6990-5p}$, $FEXO^{miR-5128-mimic}$, $FEXO^{miR-3473e-5p\text{-}mimic}$, $FEXO^{NC}$, $FEXO^{NC}$ + GPR137, GPR137 (Polyplus-transfection overexpressed group) and siGPR137 (Polyplus-transfection downregulated group). In the middle of the surgery, the mice were subcutaneously injected with 100 μl of EXO, FEXO, $FEXO^{NC}$ and $FEXO^{anti\text{-}miR-183-5p}$ at 100 μg/ml from the opposite site of skin flaps (not from the surface), whereas the mice in the PBS group were administered 100 μl of sterile PBS. The mice in the FGF1 group received 100 μl of FGF1 solution (FGF1 was obtained from the Department of Pharmacology at Wenzhou Medical University) at 15 μg/ml. Afterward, the skin flap was stretched flat, attached to the dorsal wound and sutured with 4-0 non-absorbable silk. 3-MA was administered daily for 7 days to block autophagy. Furthermore, the mice were injected daily with DMNQ, PETCM and Actin A for 7 days to activate oxidative stress, apoptosis and pyroptosis.

The percentage of survival area and the level of blood flow were measured on the 7th day following surgery. The mice were anesthetized and placed in a quiet environment. The images of skin flaps were then captured by a digital camera. ImageJ software was utilized to process the survival area and total area to calculate the percentage of survival area (percentage of survival area = survival area/total area x 100 %). Laser Doppler instruments (Moor Instruments, Axminster, UK) were used to measure the level of blood flow in skin flaps. The temperature of skin flaps was measured by an infrared thermal imager (Flir Thermal Studio). The relative temperature was determined by subtracting normal skin temperature from skin flap temperature (relative temperature = skin flap temperature-normal skin temperature). The higher negative value indicates the lower temperature of the skin flap. Statistical analysis was conducted on the average value obtained after measuring each mouse three times. RPSFs were divided into three segments of equal size based on their measurement: Area I (proximal), Area II (intermediate)

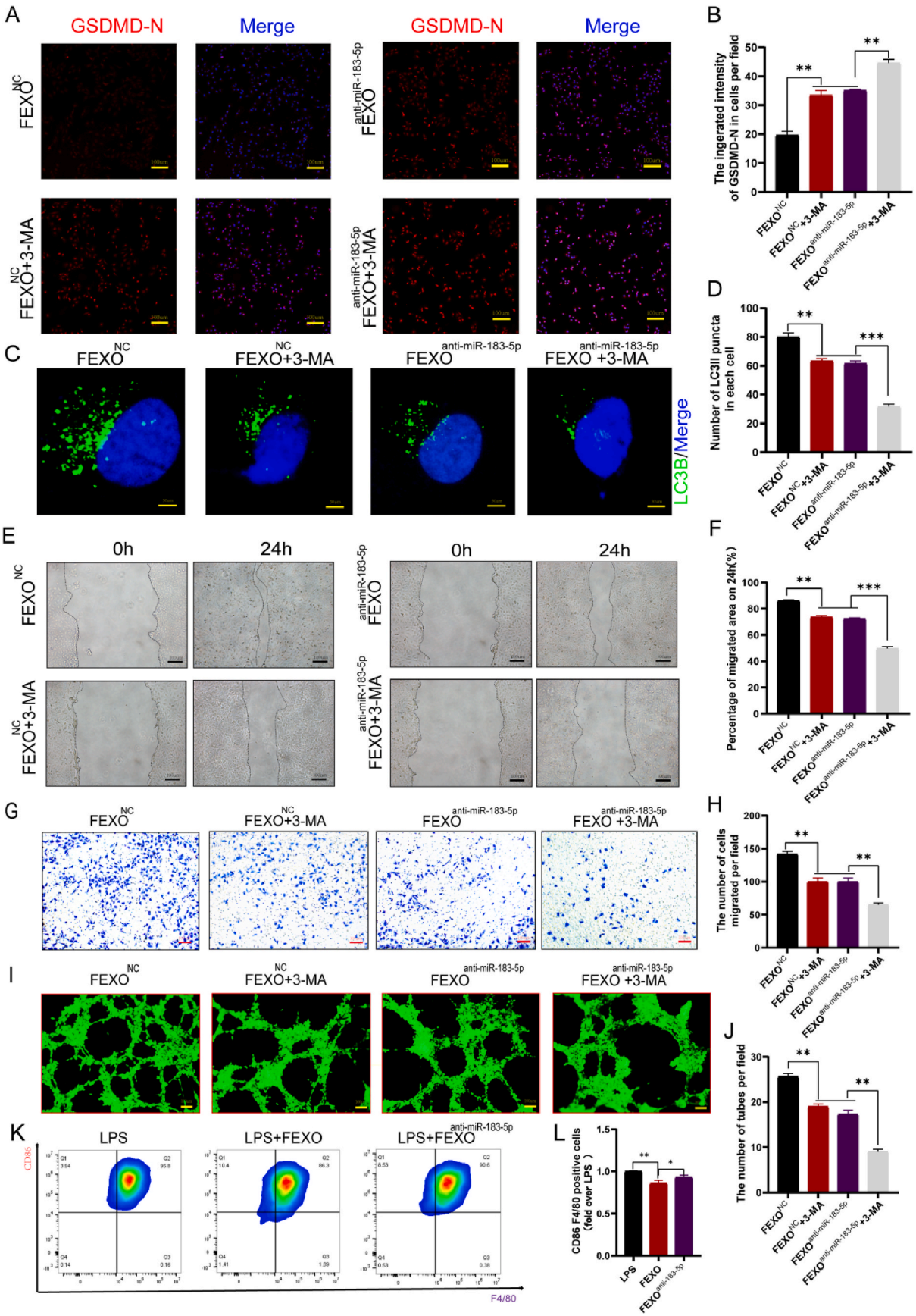

(caption on next page)

Fig. 7. Endothelial cells with exosomal miR-183-5p inhibited autophagy, viability and pyroptosis. (A) The immunofluorescence images of GSDMD-N in $FEXO^{NC}$, $FEXO^{NC}$ + 3-MA, $FEXO^{anti\text{-}miR-185-5p}$, $FEXO^{anti\text{-}miR-185-5p}$ + 3-MA and FEXO + 3-MA groups. (B) The immunofluorescence intensity of GSDMD-N was analyzed in each group (n = 3). (C) The immunofluorescence images of LC3B puncta in OGD endothelial cells. (D) The number of activated LC3B puncta in each OGD endothelial cell was calculated (n = 3). (E) The image of scratch wound assays in $FEXO^{NC}$, $FEXO^{NC}$+3-MA, $FEXO^{anti\text{-}miR-183-5p}$ and $FEXO^{anti\text{-}miR-183-5p}$+3-MA groups. (F)The percentage of migrated area by scratch wound assay was analyzed in each group (n = 3). (G) The image of the transwell assay in $FEXO^{NC}$ + 3-MA, $FEXO^{anti\text{-}miR-185-5p}$, $FEXO^{anti\text{-}miR-185-5p}$ + 3-MA and FEXO + 3-MA. (H) The number of migrated cells in each group (n = 3). (I) The image of tube formations in $FEXO^{NC}$ + 3-MA, $FEXO^{anti\text{-}miR-185-5p}$, $FEXO^{anti\text{-}miR-185-5p}$ + 3-MA and FEXO + 3-MA. (J) The number of tubes in each group (n = 3). (K–L) flow cytometry analysis and quantification of M1-like macrophage. * stands for $P < 0.05$, ** stands for $P < 0.01$, *** stands for $P < 0.001$, ns stands for not significant.

and Area III (distal). The skin samples from Area II were collected for western blot, qRT-PCR and immunofluorescence analyses.

For diabetes model, the mice were injected intraperitoneally with STZ (100 mg/kg) (Yeasen, 60256ES60) for seven days. Hyperglycemic status of mice was confirmed with blood glucose >13.8 mmol/L. After the wound surgery, 50 μl of PBS, EXO (100ug/ml), FGF (15ug/ml) or FEXO (100ug/ml) solution was pipetted dropwise to the wound bed within 30 min of preparation at D1 D3, D5, D7, D9. The images of diabetes wound were pictured by a digital camera, and analyzed by imageJ at D15.

5.3. Western blot assay

The samples from the cells and skin tissues were dissected and homogenized in ice-cold RIPA lysis solution (Beyotime) containing protease and phosphatase blockers (Sigma-Aldrich). The homogenates were adequately centrifuged at 20 000 g for 30 min at 4 °C to remove hybrids. Next, the protein concentration was determined using BCA protein assay kit (Thermo Fisher Scientific). The protein samples (30 g each) were loaded onto SDS-PAGE gels and the samples (Millipore) were then transferred to the PVDF. The membranes were adequately blocked in 5 % skimmed milk for 2 h. The membranes were then incubated with the specific primary antibodies overnight after being washed three times with TBST solution. The primary antibodies are following: VEGF (1:1000, Abcam, ab214424), LC3B (1:1000, Huabio, ET1701-65), p62 (1:1000, Proteintech, 66184-1-Ig), NLRP3 (1:1000, Proteintech, 27458-1-AP), GSDMD-N (1:1000, Affinity, DF13758), Cleaved Caspase1 (1:1000, Affinity, AF4005), GPR137 (1:1000, Proteintech, 11929-1-AP), mTOR (1:1000, Huabio, ET1608-5), P-mTOR (1:1000, Huabio, HA721632), PI3K (1:1000, Huabio, HA721673), P-PI3K (1:1000, Abclonal, AP0427), AKT (1:1000, Huabio, ET1609-51), P-AKT (1; 1000, Huabio, ET1607-73) and VAMP3 (1:1000, Abclonal, A8812), FGF1 (1:1000, Zenbio, R24301), GAPDH (1:50000, proteintech, 60004-1-IG). Next, the membranes were thoroughly washed with TBST three times and incubated with secondary antibodies conjugated to HRP for 2 h at room temperature. The intensities of band signals were finally measured using ECL immunodetection commercial kit (Biosharp) and ChemiDoc TM XRS + imaging system (Bio-Rad).

5.4. Immunofluorescence staining

The tissues obtained from Area-II of the skin flaps were fixed in 4 % paraformaldehyde. The tissues were dehydrated, embedded in paraffin and then cut into 4 μm pieces. The sections of the skin were deparaffinized using xylene. The sections were then rehydrated, washed and renatured in 10.2 mM sodium citrate buffer solution for 20 min at 95 °C. The sections were cooled to room temperature and blocked for 1 h with 3 % BSA in 1(X) PBS. Afterward, the specific primary antibodies were incubated overnight at 4 °C. The primary antibodies used in this study were CD31 (1:200, Servicebio, GB11063-1-100), EMCN (1:200, Servicebio, GB112648-100) and Cytochrome C (1:200, proteintech, 66264-1-IG), CD4 (1:200, Abclonal, A0363), Foxp3 (1:200, proteintech, 65089-1-IG). To perform cell immunofluorescence, the slides of the cells were fixed in 4 % formaldehyde for 20 min. The cells were then permeabilized for 30 min with 0.2 % Triton X-100. The slides were blocked with 3 % BSA and then incubated overnight with GSDMD-N (Affinity, DF13758, 1:200), LC3B (CST, 3868T, 1: 1600) and Cytochrome C (1:200, proteintech, 66264-1-IG). Then, the cell sections were incubated with specific secondary antibodies for 1 h at 37 °C and stained with DAPI solution. Fluorescence microscopy (Nikon, Japan) was utilized to capture the positive images.

5.5. TUNEL staining

The tissue samples from skin flaps were dehydrated in 30 % sucrose solution. The dehydrated tissues were then coated with OCT and cooled until solidified. The tissues were cut into sections of 20 mm thickness. The tissue sections were rinsed with PBS three times to remove OCT and then quickly fixed with 4 % paraformaldehyde for 15 min. Next, the tissue sections were incubated with 1 g/ml of proteinase K solution in PBS for 30 min. After that, 100 ml of equilibration buffer per slide was carefully added and incubated for another 5–10 min. Each tissue slide was then covered with 100 ml of the TdT reaction mixture and incubated at 37 °C for an additional 1 h. The tissue slides were washed in PBS and finally imaged under a fluorescence microscope. The procedure for Tunel staining was the same as described above for HUVECs.

5.6. DHE staining

The tissue samples and HUVECs, L929 and Hacat cells were processed in a similar manner for Tunel staining as well. The cells and tissue sections were co-cultured with diluted DHE solution (Beyotime) in PBS for 30 min at 37 °C. The cells were washed thrice with PBS and examined under a fluorescence microscope.

5.7. Culture of adipose-derived stem cells and isolation and identification of exosomes

The adipose stem cells (ADSCs) were purchased from OriCell (MUBMD-01001) and cultivated according to the supplier's directions. The cells were inoculated into a 25 cm^2 flask at the density of 1×10^6 cells/ml and cultured in ADSCs medium containing 10 % FBS (OriCell, MUXMD-90011) and 1 % penicillin-streptomycin (Gibco) at 37 °C. The ADSCs medium was replaced and cleansed with 10 % FBS medium (OriCell, MUXMD-90012, Exosomes free) and FGF1 (60 ng/ml) until adherent cells reached 80%–90 % confluence and cultured for 48 h.

The medium was collected and centrifuged at 300 g/min for 10 min to remove extra cells, followed by 800 g/min for 5 min at 4 °C to remove cellular debris. The supernatant was collected, centrifuged at 10000×*g* for 30 min and filtered through 0.22-μm SteritopTM sterile filter (Millipore). The filtered supernatants were then ultra-centrifuged at 100 000×*g* for 70 min at 4 °C in an Optima L-100 XP ultracentrifuge (Beckman Coulter) to obtain exosomes. After removing the supernatant, the pellets were properly washed with sterile PBS and ultra-centrifuged at 100 000×*g* for 70 min. The exosomes were finally suspended with PBS for further experiments.

We analyzed the size distribution and number of exosomes using nanoparticle flow cytometry (NanoFCM, N30E) and observed the exosome morphology using transmission electronic microscope (Hitachi, HT-7700). Bicinchoninic Acid (BCA) Protein Assay Kit (Thermo Fisher Scientific) was used to measure the concentration of exosomes. We executed the western blot technique to identify the expression of exosome-specific markers CD81 (1:1000, Abclonal, A4863), CD9 (1:1000, Abclonal, A19027) and calnexin (1:1000, BOSTER, A03372-2).

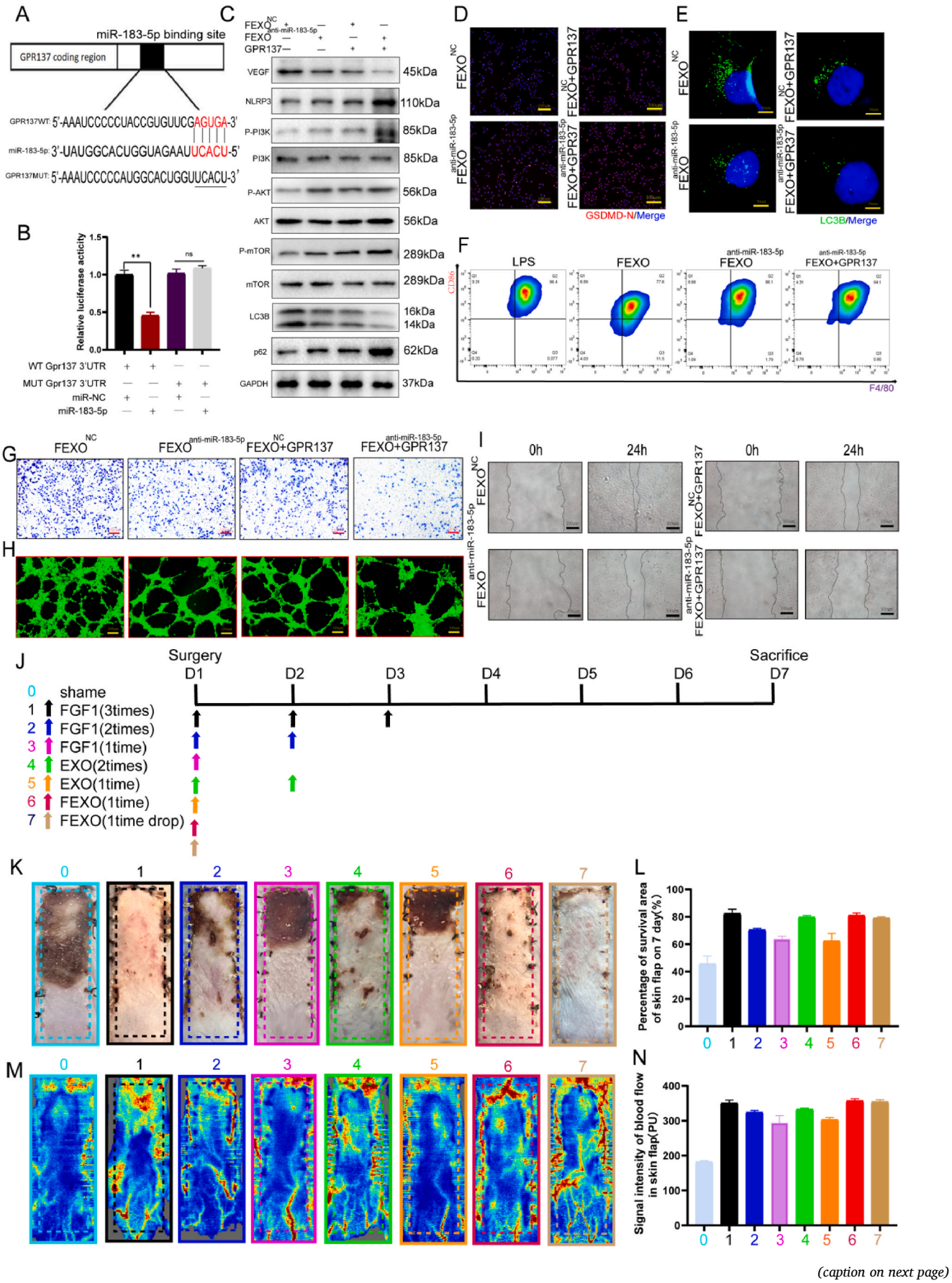

(caption on next page)

Fig. 8. Exosomal miR-183-5p regulated autophagy by targeting GPR137 through PI3K/AKT/mTOR signaling axis. (A–B) Luciferase reporter assay was performed to confirm that GPR137 is the target gene of miR-183-5p. (C) The expression of VEGF, NLRP3, P-PI3K, PI3K, P-AKT, AKT, P-mTOR, mTOR, LC3B and p62 expressions of OGD Bend3 in $FEXO^{NC}$, $FEXO^{anti\text{-}miR-183-5p}$, $FEXO^{NC}$ + GPR137 and $FEXO^{anti\text{-}miR-183-5p}$ + GPR137 group. The gels have been run under the same experimental conditions, and cropped blots were used here. (D) The immunofluorescence images of GSDMD-N in $FEXO^{NC}$, $FEXO^{anti\text{-}miR-185-5p}$, $FEXO^{NC}$ + GPR137 and $FEXO^{anti\text{-}miR-185-5p}$ + GPR137 groups. (E) The immunofluorescence images of LC3B puncta in OGD endothelial cells. (F) Flow cytometry image of M1-like macrophage. (G) The image of the transwell assay in $FEXO^{NC}$, $FEXO^{anti\text{-}miR-185-5p}$, $FEXO^{NC}$ + GPR137 and $FEXO^{anti\text{-}miR-185-5p}$ + GPR137 groups. (H) The image of tube formations in $FEXO^{NC}$, $FEXO^{anti\text{-}miR-185-5p}$, $FEXO^{NC}$ + GPR137 and $FEXO^{anti\text{-}miR-185-5p}$ + GPR137 groups. (I) The image of scratch wound assays in $FEXO^{NC}$, $FEXO^{anti-183-5p}$, $FEXO^{NC}$ + GPR137 and $FEXO^{anti\text{-}miR-183-5p}$ + GPR137 group. (J) Schematic illustration of the animal treatment protocol in the RPSFs model. (K) The image of different mice RPSFs. (L) The percentage of survival area in each group (n = 5). (M) The LDBF images of RPSFs in PBS, EXO, FEXO and FGF1 groups on D7. (N) The analysis of blood flow in each group (n = 5). * stands for $P < 0.05$, ** stands for $P < 0.01$, *** stands for $P < 0.001$, ns stands for not significant.

The exosomes were incubated in Dil solution (Beyotime) for 30 min and co-cultured with HUVECs for 12 h. Fluorescence microscopy (Nikon, Japan) was performed to observe the uptake of exosomes.

5.8. The culture of endothelial cells, L929 cells, Hacat cells and macrophage

Human umbilical vein endothelial cells (HUVECs), mouse brain-derived endothelial cells 3 (bend3), L929 and Hacat cells were obtained from the School of Pharmaceutical Sciences, Wenzhou Medical University. The cells were cultivated in an endothelial cell medium (Sciencell, NO.1001) containing 10 % FBS and 1 % penicillin-streptomycin solution (Gibco) at 37 °C in 5 % CO_2. The cells were then pre-cultured with EXO, FEXO and $FEXO^{anti\text{-}mir-183-5p}$ at a concentration of 80 g/ml for 12 h for the cell OGD model. The medium was removed and the cells were washed several times with PBS solution. The cells were then cultivated in glucose-free DMEM with EXO (80 g/ml), FEXO (80 g/ml) or $FEXO^{anti\text{-}mir-183-5p}$ (80 g/ml) for another 24 h. The culture conditions were converted to 37 °C, 0.5 % O_2, 94.5 % N_2 and 5 % CO_2. Cells were treated with 3-MA (5 mM) to block the activation of autophagy. As described previously, the bend3 cells treated with OGD were used in western blot analyses. HUVECs, L929 and Hacat cells treated with OGD were used for immunofluorescence and functional studies.

Cells were seeded onto the sterile coverslips in each 12-well culture dish containing 1 ml culture medium. After the medium was removed for immunofluorescence, the cells were fixed for 20 min at room temperature in 2 % formaldehyde. The coverslips were washed thrice by adding 1 ml PBS, pH 7.4, leaving it for 5 min and aspirating the PBS. Then, the coverslips were adequately blocked in 1(X) PBS containing 0.2 % Triton X-100 containing 3 % BSA. The coverlips were cleaned three times with PBS after being removed from the BSA and used for further experiments as described previously.

RAW264.7 macrophages were obtained from Department of Pharmacology at Wenzhou Medical University. The RAW264.7 macrophages were stimulated with LPS (Sigma Aldrich, 200 ng μg/ml) for 24 h to induce the inflammatory phenotype and then co-cultured with the different kinds of extracellular vesicles (80 μg/ml). In order to analyze the conversion of M1and M0 phenotype of RAW264.7 macrophages, single cell suspensions were incubated with F4/80- PB450, CD86-APC for 30 min at 4 °C, according to the manufacturer's instructions. All the cells were determined by a FACSVerse 8 flow cytometer, and the data were analyzed by a FlowJo software.

5.9. RNA isolation, RNA sequences and real-time quantitative PCR

Total RNA was extracted from patients and mice skin flaps and cells using Trizol reagent (Thermo Fisher Scientific) following the suppliers's dirrrections. The concentration of purified RNA was measured by NanoDrop 2000 spectrophotometer (Thermo Scientific, USA). The sequences of primers were designed by Generay Biotech and the sequences were the following : GPR137: 5′-TTGACGCTTATGAACTCTACTTT-3′ (forward),5′-CGCAGATGACGAACAGGGA-3′(reverse).GPR137B:5′-CTGCTTCCCCGTGTGTCTAC-3′(forward),5′-GCCTTGAAAAT-CACCTGCGT-3′(reverse).GPR137C:5′-CTCTTCGCCTTTGCCTACCTG-3′ (forward),5′-CAGAGCGTGGAGAACTGTAGG-3′(reverse).GPR141:5′-TGGTGGCATTTTCGTGCTTG-3′(reverse),5′-TGGCTGGGTTCTACTGGGTA-3′(reverse).GPR146:5′-GGCCTCCTGTCTGTTGTTCT-3′(reverse),5′-ACTCCATCAAAGTC-CAGCGG-3′(reverse).GPR15:5′-AGGGCAATAACCACCAAGCA-3′ (reverse),5′-GAAATCCAGCAAGAGCAACCG-3′(reverse).GPR45:5′-GCTCAGTTACCTCAAGTCTGTT-3′(reverse),5′-CAGGCACTTTAGGGAG-GATTT-3′(reverse).GPR55:5′-ACTCAAAAGTCCGCTGGGAG-3′ (reverse),5′-CTGGTTGTGCTTTCGCTTCC-3′(reverse).miR-183-5p:5′-TATGATGTGGAGGAGGTGGATGTGA-3′(forward),5′-CCTTTCATC-CAAAGGCAAAACTACAC-3′(reverse).GAPDH:5′-GGGAGC-CAAAAGGGTCATCATCTC-3′(forward)5′-CCATGCCAGT-GAGCTTCCCGTTC-3′(reverse).U5′-CTCGCTTCGGGCAGCACA-3′(for-ward),5′-AACGCTTCACGAATTTGCGT-3′(reverse).FGF1:5′-CACATT-CAGCTGCAGCTCAG-3′(forward),5′-TGCTTTCTGGCCATAGTGAGTC-3′ (reverse).FGF2:5′-GAAAAGGCAAGATGCAGGAG-3′(forward),5′-ACGT-GAGAGCAGAGCATGTG-3′(reverse).FGF9:5′-GCATCCATGGTGTGC-CAGTGAAACAGCAGA-3′(forward),5′-GTAACCATGGCA-GAGGACTCGGCTTTTGGA-3′(forward).FGF18:5′-TGCGCTTGTAC-CAGCTCTAC-3′(forward),5′-CACTCCTTGCTAGTACCATC-3′(reverse), FGF12:5′-GACGAAAACAGCGACTACACTCTC-3′(forward), CACAACTTTGCCTCCATTCATGGT-3′(reverse),FGFR1:5′-GTGTGCCTGTGGAGGAACTTT-3′(forward),5′-CTGCTTGAAGGTGGGTCTCT-3′(reverse).CD206:5′-TGGTITCCAIT-GAAAGTGCTGC-3′(forward),5′-TTCCTGGGC1TGACTGACTG1TA-3′ (reverse).si-vamp:5′-UGAGAGUCAAUGUGGAUAATT-3′(sense),5′-UUAUCCACAUUGACUCUCATT-3′(antisense),andsi-NC:5′-UUCUCC-GAACGUGUCACGUTT-3′(sense),5′-ACGUGACACGUUCGGAGAATT-3′ (antisense).VAMP1:5′-TGATCCCGCAGCTCAGTTTT-3′(reverse),5′-TCCTATCCTCGGCTCCAACA-3′(reverse).VAMP2:5′-GACTTTTGGG-GAACCAGGCT-3′(reverse),5′-CGGGGTAAGGGAAGCAAACT-3′ (reverse).VAMP3:5′-CTCACCAAGGCATCAGTCTG-3′(forward),5′-ATTC-TAAGAGCACCAGGCATC-3′(reverse).VAMP5:5′-CTGGA-CATGAGTTCGGCCTT-3′(reverse),5′-TCGGAAGAAAGACGACCAGC-3′ (reverse).VAMP8:5′-CGCCTACCTGGAGAAACCTG-3′(reverse),5′-GGGCCTCTCAAAGCAGAACT-3′(reverse).Reverse-transcription of total RNA was performed using HiScript III RT SuperMix (+gDNA wiper) (Vazyme) on the GeneAmp PCR system (Applied Biosystems). MicroRNA first-strand cDNA was constructed using the miRNA cDNA synthesis kit (Vazyme). The quantitative PCR was carried out using Taq Pro Universal SYBR qPCR Master Mix (Vazyme) and C1000 Touch Thermal Cycler (BIO-RAD, USA). Transcriptome sequencing and analysis of FEXO v EXO was carried out by 10K Genomics (Shanghai, China).

5.10. Plasmids and transfection

Mir-183-5p and miR-6990-5p antigomirs, miR-5128, miR-3473e and miR-3473b mimics, plasmids for GPR137 expression, siGPR137 and siVamp3 oligonucleotides (Hunan Fenghui Biotechnology Co., Ltd) were transfected into ADSCs, HUVECs and bend 3 cells with transfection reagents (Thermo Fisher Scientific). The cells were used for subsequent experiments after 24 h of transfection. The GPR137 expression plasmids and siGPR137 were applied directly to the mouse skin using vivo-jetPEI (201-10G, Polyplus-transfection, Illkirch) as instructed by the manufacturer.

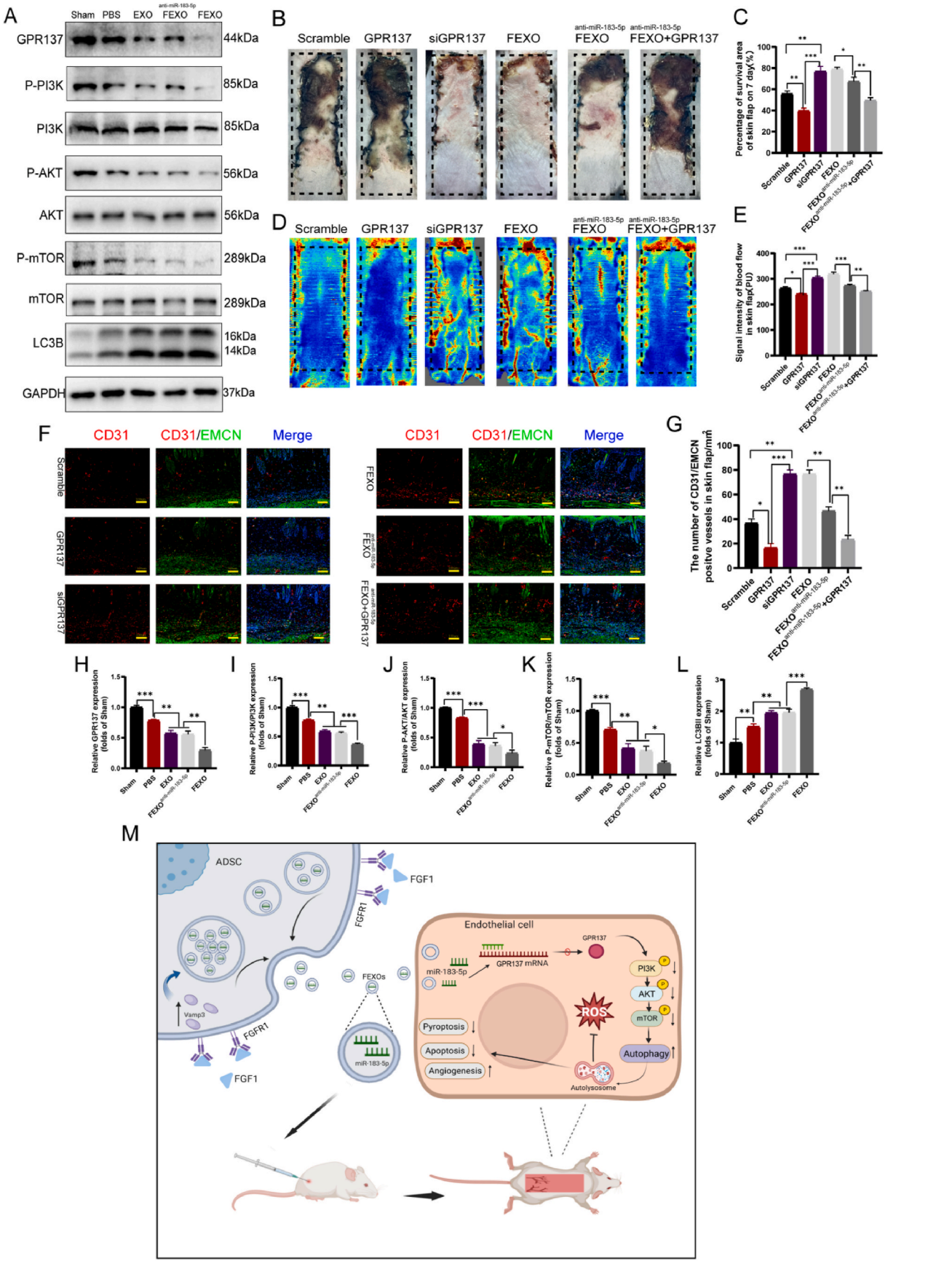

(caption on next page)

Fig. 9. GPR137 might be a new therapeutic target for random-pattern skin flaps. (A)The expression of GPR137, P-PI3K, PI3K, P-AKT, AKT, P-mTOR, mTOR and LC3B expressions of RPSFs in the Shame, PBS, EXO, FEXO$^{anti\text{-}miR-183-5p}$, FEXO groups. The gels have been run under the same experimental conditions, and cropped blots were used here. (B) Digital image of RPSFs on D7 in Scramble, GPR137, siGPR137, FEXO, FEXO$^{anti\text{-}miR-183-5p}$ and FEXO$^{anti\text{-}miR-183-5p}$ + GPR137 groups. (C) The percentage of survival area in each group (n = 5). (D) The full field LDBF images of RPSHs in Scramble, GPR137, siGPR137, FEXO, FEXO$^{anti\text{-}miR-183-5p}$ and FEXO$^{anti\text{-}miR-183-5p}$ + GPR137 groups on D7. (E) The signal intensity of blood flow of flaps was analyzed in each group (n = 5). (F) The immunofluorescence images of CD31/EMCN positive vessels of skin flaps in Scramble, GPR137, siGPR137, FEXO, FEXO$^{anti\text{-}miR-183-5p}$ and FEXO$^{anti\text{-}miR-183-5p}$ + GPR137 groups. (G) The number of CD31/EMCN positive vessels were analyzed in each group (n = 3). (H–L) The density value of the proteins in OGD endothelial cells in each group (n = 3). (M) The graphical abstract of extracellular vesicles containing miR-183-5p derived from FGF1-pretreated ADSCs protect endothelial cells from oxidative stress, apoptosis and pyroptosis through enhancing autophagy.

5.11. Luciferase reporter assay

Luciferase reporter plasmids containing the wild-type or mutant GPR137 3′UTR (Hunan Fenghui Biotechnology Co., Ltd) were cotransfected with bend3 cells to derive the reporter zygotes. The relative luciferase activity of the cells was determined using dual luciferase reporter assay kit (Solarbio, D0011), according to the supplier's instructions.

5.12. Cell migration assay

Transwell cell migration assay was developed to analyze the migration of HUVECs through Corning Transwell® (8.0 mm polycarbonate membrane). HUVECs were seeded into the upper chambers (1x106 cells per chamber) and incubated at 37 °C, 0.5 % O_2, 94.5 % N_2 and 5 % CO_2 for 24 h with 1 % FBS-containing culture medium and the 24-well culture dish filled with 10 % FBS-containing culture medium. The cells were then fixed with 4 % paraformaldehyde and stained with crystal violet (Beyotime) and the migrated cells were visualized by a computerized microscope.

5.13. Scratch wound assay

HUVECs were seeded in six-well culture dishes filled with a pipette tip for scratch wound assays. The dish was gently washed to remove detached cells and fresh culture medium was added to the liquid. The dishes were then incubated at 37 °C, 0.5 % O_2, 94.5 % N_2 and 5 % CO_2 for 24 h. The scratch wound assay was finally analyzed with a computer-aided microscope.

5.14. Tube formation

HUVECs were stained with Calcein AM dye (Beyotime) for 30 min and plated on BeyoGoldTM 35 mm Confocal Dishes (Beyotime). The dishes were pre-filled with growth factor-reduced Matrigel. The formation of capillary-like tubes was finally observed in a computer-assisted microscope after 4 h of incubation at 37 °C and 0.5 % O_2.

5.15. Statistical analysis

The experiments were randomized and blinded. All the experimental data are expressed as the mean ± standard error of the mean (SEM). The number of experimental groups/conditions (n) is indicated for each group and n refers to independent values (not replicates). All data used in the present study were normalized. The statistical analyses were performed using SPSS software version 19 (Chicago, IL, USA). Post-hoc analyses were performed using an independent-sample *t*-test, a one-way ANOVA with LSD (equal variances assumed) or Dunnett's T3 (equal variances not assumed). P-values <0.05 were considered statistically significant. This standard deviation was applied to * $P < 0.05$, ** stands for $P < 0.01$, *** stands for $P < 0.001$ and ns stands for not significant.

CRediT authorship contribution statement

Xuanlong Zhang: Writing – original draft, Visualization, Software, Methodology, Investigation. **Xiaoqiong Jiang:** Methodology, Investigation, Funding acquisition. **Huiming Deng:** Software, Methodology, Investigation. **Gaoxiang Yu:** Methodology, Investigation. **Ningning Yang:** Software, Methodology, Investigation. **Abdullah Al Mamun:** Software, Methodology, Investigation. **Feifei Lian:** Methodology, Formal analysis. **Tianling Chen:** Methodology, Investigation. **Haijuan Zhang:** Resources, Methodology, Investigation. **Yingying Lai:** Methodology, Investigation. **Jiayi Huang:** Investigation, Formal analysis. **Shi Xu:** Methodology. **Fuman Cai:** Writing – review & editing. **Xiaokun Li:** Writing – review & editing. **Kailiang Zhou:** Writing – review & editing. **Jian Xiao:** Writing – review & editing, Funding acquisition.

Declaration of competing interest

The authors declare that they have no known competing financial interests or personal relationships that could have appeared to influence the work reported in this paper.

Acknowledgment

This research was supported by the Key Scientific and Technological Innovation Projects of Wenzhou (ZY20200023), the National Natural Science Foundation of China (82172428), the Basic Public Welfare Research Project of Zhejiang Province (LGF22H110002), Zhejiang Provincial Natural Science Foundation of China (LZ23H060001). The diagram of the Potential underlying mechanism was supported by the Biorender app (https://app.biorender.com).

Appendix A. Supplementary data

Supplementary data to this article can be found online at https://doi.org/10.1016/j.mtbio.2024.101314.

Data availability

Data will be made available on request.

References

[1] Y. Wu, J. Peng, X. Luo, T. Wang, The application of modified kite flap in repairing facial skin defects after tumor resection, Ann. Plast. Surg. 88 (2022) 59, https://doi.org/10.1097/SAP.0000000000003008.
[2] S.S. Nagel, B. Thomas, S. Fischer, Y. Diehm, B. Ziegler, A.K. Bigdeli, V.J. Schmidt, U. Kneser, C.A. Radu, Random-pattern versus perforator-based adipocutaneous skin paddles for postoperative monitoring of free muscle flaps-a comparative retrospective cohort study, J Plast Reconstr Aesthet Surg 74 (2021) 747, https://doi.org/10.1016/j.bjps.2020.10.016.
[3] R. Ogawa, Head and neck reconstruction in burn patients, Clin. Plast. Surg. 51 (2024) 391, https://doi.org/10.1016/j.cps.2024.02.003.
[4] A.M. Carvalho Brinca, A. de Castro Pinho, R.J.D. Costa Vieira, Blood perfusion of random skin flaps in humans-in vivo assessment by laser speckle contrast imaging, Dermatol. Surg. 47 (2021) 1421, https://doi.org/10.1097/DSS.0000000000003164.
[5] L. Lyu, H. Kim, J.S. Bae, C. Hua, J.H. Kim, E.H. Kim, J.H. Mo, I. Park, The application of SFDI and LSI system to evaluate the blood perfusion in skin flap mouse model, Lasers Med Sci. 37 (2022) 1069, https://doi.org/10.1007/s10103-021-03354-6.
[6] C.C. Hsu, C.Y.Y. Loh, F.C. Wei, The anterolateral thigh perforator flap: its expanding role in lower extremity reconstruction, Clin. Plast. Surg. 48 (2021) 235, https://doi.org/10.1016/j.cps.2020.12.008.

[7] S.D. Kozusko, X. Liu, C.A. Riccio, J. Chang, L.C. Boyd, Z. Kokkalis, P. Konofaos, Selecting a free flap for soft tissue coverage in lower extremity reconstruction, Injury 50 (2019) S32, https://doi.org/10.1016/j.injury.2019.10.045.

[8] K.T. Mankin, Axial pattern flaps, Vet Clin North Am Small Anim Pract. 47 (2017) 1237, https://doi.org/10.1016/j.cvsm.201.

[9] J. Lou, H. Zhang, J. Qi, Y. Xu, X. Wang, J. Jiang, X. Hu, L. Ni, Y. Cai, X. Wang, W. Gao, J. Xiao, K. Zhou, Cyclic helix B peptide promotes random-pattern skin flap survival via TFE3-mediated enhancement of autophagy and reduction of ROS levels, Br. J. Pharmacol. 179 (2022) 301, https://doi.org/10.1080/15548627.2021.2002109.

[10] L. Song, L. Mu, H. Wang, MicroRNA-489-3p aggravates neuronal apoptosis and oxidative stress after cerebral ischemia-reperfusion injury, Bioengineered 13 (2022) 14047, https://doi.org/10.1080/21655979.2022.2062534.

[11] K. Odake, M. Tsujii, T. Iino, K. Chiba, T. Kataoka, A. Sudo, Febuxostat treatment attenuates oxidative stress and inflammation due to ischemia-reperfusion injury through the necrotic pathway in skin flap of animal model, Free Radic. Biol. Med. 177 (2021) 238, https://doi.org/10.1016/j.freeradbiomed.

[12] W.T. Yan, Y.D. Yang, X.M. Hu, W.Y. Ning, L.S. Liao, S. Lu, W.J. Zhao, Q. Zhang, K. Xiong, Do pyroptosis, apoptosis, and necroptosis (PANoptosis) exist in cerebral ischemia? Evidence from cell and rodent studies, Neural Regen Res 17 (2022) 1761, https://doi.org/10.4103/1673-5374.331539.

[13] Z. Rao, Y. Zhu, P. Yang, Z. Chen, Y. Xia, C. Qiao, W. Liu, H. Deng, J. Li, P. Ning, Z. Wang, Pyroptosis in inflammatory diseases and cancer, Theranostics. 12 (2022) 4310, https://doi.org/10.7150/thno.71086.

[14] S. Li, Y. Sun, M. Song, Y. Song, Y. Fang, Q. Zhang, X. Li, N. Song, J. Ding, M. Lu, G. Hu, NLRP3/caspase-1/GSDMD-mediated Pyroptosis Exerts a Crucial Role in Astrocyte Pathological Injury in Mouse Model of Depression, vol. 6, 2021 146852, https://doi.org/10.1172/jci.insight.146852.

[15] H. Cao, J. Liang, J. Liu, Y. He, Y. Ke, Y. Sun, S. Jiang, J. Lin, Novel effects of combination therapy through inhibition of caspase-1/gasdermin D induced-pyroptosis in lupus nephritis, Front. Immunol. 12 (2021) 720877, https://doi.org/10.3389/fimmu.2021.720877.

[16] K. Gumpper-Fedus, K.H. Park, H. Ma, X. Zhou, Z. Bian, K. Krishnamurthy, M. Sermersheim, J. Zhou, T. Tan, L. Li, J. Liu, P.H. Lin, H. Zhu, J. Ma, MG53 preserves mitochondrial integrity of cardiomyocytes during ischemia reperfusion-induced oxidative stress, Redox Biol. 54 (2022) 102357, https://doi.org/10.1016/j.redox.2022.102357.

[17] H.A. Kalpage, V. Bazylianska, M.A. Recanati, A. Fite, J. Liu, J. Wan, N. Mantena, M.H. Malek, I. Podgorski, E.I. Heath, A. Vaishnav, B.F. Edwards, L.I. Grossman, T. H. Sanderson, I. Lee, M. Hüttemann, Tissue-specific regulation of cytochrome c by post-translational modifications: respiration, the mitochondrial membrane potential, ROS, and apoptosis, FASEB J. 33 (2019) 1540, https://doi.org/10.1096/fj.201801417R.

[18] A.R. Baek, J. Hong, K.S. Song, A.S. Jang, D.J. Kim, S.S. Chin, S.W. Park, Spermidine attenuates bleomycin-induced lung fibrosis by inducing autophagy and inhibiting endoplasmic reticulum stress (ERS)-induced cell death in mice, Exp. Mol. Med. 52 (2020) 2034, https://doi.org/10.1038/s12276-020-00545-z.

[19] W. Chen, Y. Chen, Y. Liu, X. Wang, Autophagy in muscle regeneration: potential therapies for myopathies, J Cachexia Sarcopenia Muscle 13 (2022) 1673, https://doi.org/10.1002/jcsm.13000.

[20] X. Chen, G. Tong, J. Fan, Y. Shen, N. Wang, W. Gong, Z. Hu, K. Zhu, X. Li, L. Jin, W. Cong, J. Xiao, Z. Zhu, FGF21 promotes migration and differentiation of epidermal cells during wound healing via SIRT1-dependent autophagy, Br. J. Pharmacol. 179 (2022) 1102, https://doi.org/10.1111/bph.15701.

[21] M. Zakrzewska, E. Marcinkowska, A. Wiedlocha, FGF-1: from biology through engineering to potential medical applications, Crit. Rev. Clin. Lab Sci. 45 (2008) 91, https://doi.org/10.1080/10408360701713120.

[22] M. Mollapour Sisakht, F. Gholizadeh, Z. Shahravi, Y. Kiani Doust-Vaghe, M. A. Nilforoushzadeh, M.A. Amirkhani, Sodium alginate/polyacrylic acid hydrogel composite, potential carrier for fibroblast growth factor1 (FGF1) delivery, Chem. Biodivers. 27 (2024) e202401738.

[23] R. Böhm, E. Proksch, T. Schwarz, I. Cascorbi, Drug hypersensitivity, Dtsch Arztebl Int 115 (2018) 501, https://doi.org/10.3238/arztebl.2018.0501.

[24] H. Akbari, M. Ahmadi, M.J. Fatemi, A. Foroutan, P. Akbari, H. Bagheri, M. Golkar, The role of recombinant fibroblast growth factor 1 in enhancing the angiogenesis in random cutaneous flaps in animal model of rat, World J. Plast. Surg. 10 (2021) 76, https://doi.org/10.29252/wjps.10.2.76.

[25] Z. Chen, M. Jin, H. He, J. Dong, J. Li, J. Nie, Z. Wang, J. Xu, F. Wu, Mesenchymal stem cells and macrophages and their interactions in tendon-bone healing, J Orthop Translat 39 (2023) 63, https://doi.org/10.1016/j.jot.2022.12.005.

[26] S Zhao, Q Zhang, M Liu, J Du, T Wang, Y Li, W Zeng, Application of stem cells in engineered vascular graft and vascularized organs, Semin Cell Dev Biol 144 (2023) 31, https://doi.org/10.1016/j.semcdb.2022.10.003.

[27] K. Drela, L. Stanaszek, A. Nowakowski, Z. Kuczynska, B. Lukomska, Experimental strategies of mesenchymal stem cell propagation: adverse events and potential risk of functional changes, Stem Cells Int. 2019 (2019) 7012692, https://doi.org/10.1155/2019/7012692.

[28] J.O. Jeong, J.W. Han, J.M. Kim, H.J. Cho, C. Park, N. Lee, D.W. Kim, Y.S. Yoon, Malignant tumor formation after transplantation of short-term cultured bone marrow mesenchymal stem cells in experimental myocardial infarction and diabetic neuropathy, Circ. Res. 108 (2011) 1340, https://doi.org/10.1161/CIRCRESAHA.110.239848.

[29] S.V. Krylova, D. Feng, The machinery of exosomes: biogenesis, release, and uptake, Int. J. Mol. Sci. 24 (2023) 1337, https://doi.org/10.3390/ijms24021337.

[30] M.E. Al-Masawa, M.A. Alshawsh, C.Y. Ng, A.M.H. Ng, J.B. Foo, U. Vijakumaran, R. Subramaniam, N.A.A. Ghani, K.W. Witwer, J.X. Law, Efficacy and safety of small extracellular vesicle interventions in wound healing and skin regeneration: a systematic review and meta-analysis of animal studies, Theranostics 12 (2022) 6455, https://doi.org/10.7150/thno.73436.

[31] E. Fayazzadeh, H. Yavarifar, S.R. Rafie, S. Motamed, M. Sotoudeh Anvari, M. A. Boroumand, Fibroblast growth factor-1 vs. Fibroblast growth factor-2 in ischemic skin flap survival in a rat animal model, World J. Plast. Surg. 5 (3) (2016 Sep) 274–279. PMID: 27853691.

[32] S. Mishima, M. Sakamoto, H. Kioka, Y. Nagata, R. Suzuki, Multifunctional regulation of VAMP3 in exocytic and endocytic pathways of RBL-2H3 cells, Front. Immunol. 13 (2022) 885868, https://doi.org/10.3389/fimmu.2022.885868.

[33] Bajestani A. Keifi, M.S. Alavi, L. Etemad, A. Roohbakhsh, Role of orphan G-protein coupled receptors in tissue ischemia: a comprehensive review, Eur. J. Pharmacol. 978 (2024) 176762, https://doi.org/10.1016/j.ejphar.2024.176762.

[34] S. Tsuji, S. Ichioka, N. Sekiya, T. Nakatsuka, Analysis of ischemia-reperfusion injury in a microcirculatory model of pressure ulcers, Wound Repair Regen. 13 (2) (2005 Mar-Apr) 209–215, https://doi.org/10.1111/j.1067-1927.2005.130213.x.

[35] J. Lee, M. Blaber, The Interaction between Thermodynamic Stability and Buried Free Cysteines in Regulating the Functional Half-Life of Fibroblast Growth Factor-1, vol. 393, 2009, p. 113, https://doi.org/10.1016/j.jmb.2009.08.026.

[36] J. Lou, X. Wang, H. Zhang, G. Yu, J. Ding, X. Zhu, Y. Li, Y. Wu, H. Xu, H. Xu, W. Gao, J. Xiao, K. Zhou, Inhibition of PLA2G4E/cPLA2 promotes survival of random skin flaps by alleviating Lysosomal membrane permeabilization-Induced necroptosis, Autophagy 18 (2022) 1841, https://doi.org/10.1080/15548627.2021.2002109.

[37] X. Xia, L.M. Longo, M. Blaber, Mutation choice to eliminate buried free cysteines in protein therapeutics, J Pharm Sci 104 (2015) 566, https://doi.org/10.1002/jps.24188.

[38] D. Bian, Y. Wu, G. Song, R. Azizi, A. Zamani, The application of mesenchymal stromal cells (MSCs) and their derivative exosome in skin wound healing: a comprehensive review, Stem Cell Res. Ther. 13 (2022) 24, https://doi.org/10.1186/s13287-021-02697-9.

[39] Y. Liang, L. Duan, J. Lu, J. Xia, Engineering exosomes for targeted drug delivery, Theranostics 11 (2021) 3183, https://doi.org/10.7150/thno.52570.

[40] O.M. Elsharkasy, J.Z. Nordin, D.W. Hagey, O.G. de Jong, R.M. Schiffelers, S. E. Andaloussi, P. Vader, Extracellular vesicles as drug delivery systems: why and how? Adv. Drug Deliv. Rev. 159 (2020) 332, https://doi.org/10.1016/j.addr.2020.04.004.

[41] S.V. Krylova, D. Feng, The machinery of exosomes: biogenesis, release, and uptake, Int. J. Mol. Sci. 24 (2023) 1337, https://doi.org/10.3390/ijms24021337.

[42] R. Kalluri, V.S. LeBleu, The biology, function, and biomedical applications of exosomes, Science 367 (2020) 6977, https://doi.org/10.1126/science.aau6977.

[43] Z. Chen, H. Wu, J. Yang, B. Li, J. Ding, S. Cheng, N. Bsoul, C. Zhang, J. Li, H. Liu, D. Lin, W. Gao, Activating Parkin-dependent mitophagy alleviates oxidative stress, apoptosis, and promotes random-pattern skin flaps survival, Commun. Biol. 5 (2022) 616, https://doi.org/10.1038/s42003-022-03556-w.

[44] Z. Meng, K. Wang, Q. Lan, T. Zhou, Y. Lin, Z. Jiang, J. Chen, Y. Lin, X. Liu, H. Lin, D. Lin, Saxagliptin promotes random skin flap survival, Int Immunopharmacol 120 (2023) 110364, https://doi.org/10.1016/j.intimp.2023.110364.

[45] H.H. Pulkkinen, M. Kiema, J.P. Lappalainen, A. Toropainen, M. Beter, A. Tirronen, L. Holappa, H. Niskanen, M.U. Kaikkonen, S. Ylä-Herttuala, J. P. Laakkonen, BMP6/TAZ-Hippo signaling modulates angiogenesis and endothelial cell response to VEGF, Angiogenesis 24 (2021) 129, https://doi.org/10.1007/s10456-020-09748-4.

[46] Y.H. Liu, L.M. Brunner, J. Rebling, Greenwald M. Ben-Yehuda, S. Werner, M. Detmar, D. Razansky, Non-invasive longitudinal imaging of VEGF-induced microvascular alterations in skin wounds, Theranostics 12 (2022) 558, https://doi.org/10.7150/thno.65287.

[47] Y.H. Zheng, L.Q. Yin, H.K. Xu, X. Gong, Non-invasive physical therapy as salvage measure for ischemic skin flap: a literature review, World J Clin Cases 9 (2021) 3227, https://doi.org/10.12998/wjcc.v9.i14.3227.

[48] A. Cruz-Segura, M.P. Cruz-Domínguez, L.J. Jara, Á. Miliar-García, A. Hernández-Soler, P. Grajeda-López, M.A. Martínez-Bencomo, D.H. Montes-Cortés, Early detection of vascular obstruction in microvascular flaps using a thermographic camera, J. Reconstr. Microsurg. 35 (2019) 541, https://doi.org/10.1055/s-0039-1688749.

[49] G. Yu, Y. Chen, N. Yang, H. Zhang, X. Zhang, Y. Geng, J. Zhao, Z. Chen, C. Dong, L. Lin, J. Qi, X. Zhang, X. Jiang, W. Gao, Y. Cai, X. Wang, J. Ding, J. Xiao, K. Zhou, Apoptotic bodies derived from fibroblast-like cells in subcutaneous connective tissue inhibit ferroptosis in ischaemic flaps via the miR-339-5p/KEAP1/nrf2 Axis, Adv. Sci. 11 (2024) e2307238, https://doi.org/10.1002/advs.202307238.

[50] G.K. Chaseling, C.G. Crandall, D. Gagnon, Skin blood flow measurements during heat stress: technical and analytical considerations, Am. J. Physiol. Regul. Integr. Comp. Physiol. 318 (2020) 57, https://doi.org/10.1152/ajpregu.00177.2019.

[51] L. Liu, C.X. Zheng, N. Zhao, T. Zhu, C.B. Hu, N. Zhang, J. Chen, K.C. Zhang, S. Zhang, J.X. Liu, K. Zhang, H. Jing, B.D. Sui, Y. Jin, F. Jin, Mesenchymal stem cell aggregation-released extracellular vesicles induce CD31+ EMCN+ vessels in skin regeneration and improve diabetic wound healing, Adv Healthc Mater 12 (2023) 2300019, https://doi.org/10.1002/adhm.202300019.

[52] X. Wei, F. Xie, X. Zhou, Y. Wu, H. Yan, T. Liu, J. Huang, F. Wang, F. Zhou, L. Zhang, Role of pyroptosis in inflammation and cancer, Cell. Mol. Immunol. 19 (2022) 971, https://doi.org/10.1038/s41423-022-00905-x.

[53] J.P. Borges, R.S.R. Sætra, A. Volchuk, M. Bugge, P. Devant, B. Sporsheim, B. R. Kilburn, C.L. Evavold, J.C. Kagan, N.M. Goldenberg, T.H. Flo, B.E. Steinberg, Glycine inhibits NINJ1 membrane clustering to suppress plasma membrane

rupture in cell death, Elife 11 (2022) 78609, https://doi.org/10.7554/eLife.78609.
[54] M. Dambrova, C.J. Zuurbier, V. Borutaite, E. Liepinsh, M. Makrecka-Kuka, Energy substrate metabolism and mitochondrial oxidative stress in cardiac ischemia/reperfusion, Injury 165 (2021) 24, https://doi.org/10.1016/j.freeradbiomed.2021.01.036.
[55] B. Wang, H. Xu, J. Kong, D. Liu, W. Qin, W. Bai, Krüppel-like factor 15 reduces ischemia-induced apoptosis involving regulation of p38/MAPK signaling, Hum. Gene Ther. 32 (2021) 1471, https://doi.org/10.1089/hum.2021.075.
[56] L. Yu, Y. Chen, S.A. Tooze, Autophagy pathway: cellular and molecular mechanisms, Autophagy 14 (2018) 207, https://doi.org/10.1080/15548627.2017.1378838.
[57] B. Levine, G. Kroemer, Biological functions of autophagy genes: a disease perspective, Cell 176 (2019) 11, https://doi.org/10.1016/j.cell.2018.09.048.
[58] Y. He, Q. Li, F. Feng, R. Gao, H. Li, Y. Chu, S. Li, Y. Wang, R. Mao, Z. Ji, Y. Hua, J. Shen, Z. Wang, M. Zhao, Q. Yao, Extracellular vesicles produced by human-induced pluripotent stem cell-derived endothelial cells can prevent arterial stenosis in mice via autophagy regulation, Front Cardiovasc Med 9 (2022) 922790, https://doi.org/10.3389/fcvm.2022.922790.
[59] L. Devis-Jauregui, N. Eritja, M.L. Davis, X. Matias-Guiu, D. Llobet-Navàs, Autophagy in the physiological endometrium and cancer, Autophagy 17 (2021) 1077, https://doi.org/10.1080/15548627.2020.1752548.
[60] S. Ciotti, L. Iuliano, S. Cefalù, M. Comelli, I. Mavelli, E. Di Giorgio, C. Brancolini, GSK3β is a key regulator of the ROS-dependent necrotic death induced by the quinone DMNQ, Cell Death Dis. 11 (2020) 2, https://doi.org/10.1038/s41419-019-2202-0.
[61] S. Ruan, C. Han, Y. Sheng, J. Wang, X. Zhou, Q. Guan, W. Li, C. Zhang, Y. Yang, Antcin A alleviates pyroptosis and inflammatory response in Kupffercells of non-alcoholic fatty liver disease by targeting NLRP3, Int Immunopharmacol 100 (2021) 108126, https://doi.org/10.1016/j.intimp.2021.108126.
[62] P. Imbriani, A. Tassone, M. Meringolo, G. Ponterio, G. Madeo, A. Pisani, P. Bonsi, Loss of non-apoptotic role of caspase-3 in the PINK1 mouse model of Parkinson's disease, Int. J. Mol. Sci. 20 (2019) 3407, https://doi.org/10.3390/ijms20143407.
[63] P.T.B. Ho, I.M. Clark, L.T.T. Le, MicroRNA-based diagnosis and therapy, Int. J. Mol. Sci. 23 (2022) 7167, https://doi.org/10.3390/ijms23137167.
[64] K. Saliminejad, H.R. Khorram Khorshid, S. Soleymani Fard, S.H. Ghaffari, An overview of microRNAs: biology, functions, therapeutics, and analysis methods, J. Cell. Physiol. 234 (2019) 5451, https://doi.org/10.1002/jcp.27486.
[65] C. Voelz, N. Ebrahimy, W. Zhao, P. Habib, A. Zendedel, T. Pufe, C. Beyer, A. Slowik, Transient focal cerebral ischemia leads to miRNA alterations in different brain regions, blood serum, liver, and spleen, Int. J. Mol. Sci. 23 (2021) 161, https://doi.org/10.3390/ijms23010161.
[66] X. Wang, S. Chen, J. Ni, J. Cheng, J. Jia, X. Zhen, miRNA-3473b contributes to neuroinflammation following cerebral ischemia, Cell Death Dis. 9 (2018) 11, https://doi.org/10.1038/s41419-017-0014-7.
[67] H. Zhu, J. Shi, W. Li, Bioinformatics analysis of ceRNA network of autophagy-related genes in pediatric asthma, Medicine (Baltim.) 102 (2023) e36343, https://doi.org/10.1097/MD.0000000000036343.
[68] S. Liang, X. Li, C. Gao, L. Zhang, microRNA-based autophagy inhibition as targeted therapy in pancreatic cancer, Biomed. Pharmacother. 132 (2020 Dec) 110799, https://doi.org/10.1016/j.biopha.2020.110799.
[69] J.J. Lin, R. Chen, L.Y. Yang, M. Gong, M.Y. Du, S.Q. Mu, Z.A. Jiang, H.H. Li, Y. Yang, X.H. Wang, S.F. Wang, K.X. Liu, S.H. Cao, Z.Y. Wang, A.Q. Zhao, S. Y. Yang, C. Li, S.G. Sun, Hsa_circ_0001402 alleviates vascular neointimal hyperplasia through a miR-183-5p-dependent regulation of vascular smooth muscle cell proliferation, migration, and autophagy, J. Adv. Res. 25 (2023) S2090, https://doi.org/10.1016/j.jare.2023.07.010.
[70] S. Zheng, Y.F. Zhong, D.M. Tan, Y. Xu, H.X. Chen, D. Wang, miR-183-5p enhances the radioresistance of colorectal cancer by directly targeting ATG5, J Biosci. 44 (2019) 92. PMID: 31502570.
[71] Y.X. Tao, Molecular chaperones and G protein-coupled receptor maturation and pharmacology, Mol. Cell. Endocrinol. 511 (2020) 110862, https://doi.org/10.1016/j.mce.2020.110862.
[72] K. Iwasa, A. Yamagishi, S. Yamamoto, C. Haruta, K. Maruyama, K. Yoshikawa, GPR137 inhibits cell proliferation and promotes neuronal differentiation in the Neuro2a cells, Neurochem. Res. 48 (2023) 996, https://doi.org/10.1007/s11064-022-03833-4.
[73] J. Lu, F. Zhong, B. Sun, C. Wang, GPR137 is a promising novel bio-marker for the prognosis of bladder cancer patients, Medicine (Baltim.) 98 (2019) 16576, https://doi.org/10.1097/MD.0000000000016576.
[74] L. Li, C. Zhu, Q. Xu, S. Xu, J. Ye, D. Xu, L. Wang, S. Gan, B. Liu, C. Tang, ALKBH1 contributes to renal cell carcinoma progression by reducing N6-methyladenine of GPR137, Eur. J. Clin. Invest. 53 (2023) 13986, https://doi.org/10.1111/eci.13986.
[75] D. Miricescu, A. Totan, I.I. Stanescu-Spinu, S.C. Badoiu, C. Stefani, M. Greabu, PI3K/AKT/mTOR signaling pathway in breast cancer: from molecular landscape to clinical aspects, Int. J. Mol. Sci. 22 (2020) 173, https://doi.org/10.3390/ijms22010173.
[76] D. Dong, J. Wu, L. Sheng, X. Gong, Z. Zhang, C. Yu, FUNDC1 induces apoptosis and autophagy under oxidative stress via PI3K/Akt/mTOR pathway in cataract lens cells, Curr. Eye Res. 47 (2022) 547, https://doi.org/10.1080/02713683.2021.2021586.
[77] G. Rizzo, J. Gropper, M. Piollet, E. Vafadarnejad, A. Rizakou, S.R. Bandi, P. Arampatzi, T. Krammer, N. DiFabion, O. Dietrich, A.P. Arias-Loza, M. Prinz, M. Mack, K. Schlepckow, C. Haass, J.S. Silvestre, A. Zernecke, A.E. Saliba, C. Cochain, Dynamics of monocyte-derived macrophage diversity in experimental myocardial infarction, Cardiovasc. Res. 119 (2023) 772, https://doi.org/10.1093/cvr/cvac113.
[78] S.L. Li, Z.M. Wang, C. Xu, F.H. Che, X.F. Hu, R. Cao, Y.N. Xie, Y. Qiu, H.B. Shi, B. Liu, C. Dai, J. Yang, Liraglutide attenuates hepatic ischemia-reperfusion injury by modulating macrophage polarization, Front. Immunol. 13 (2022) 869050, https://doi.org/10.3389/fimmu.2022.869050.
[79] W.S. Lee, K.H. Nam, J.H. Kim, W.J. Kim, J.E. Kim, E.C. Shin, G.R. Kim, J.M. Choi, Alleviating psoriatic skin inflammation through augmentation of Treg cells via CTLA-4 signaling peptide, Front. Immunol. 25 (2023) 14, https://doi.org/10.3389/fimmu.2023.1233514.
[80] J. Luan, C. Truong, A. Vuchkovska, W. Guo, J. Good, B. Liu, A. Gang, N. Infarinato, K. Stewart, L. Polak, H.A. Pasolli, E. Andretta, A.Y. Rudensky, E. Fuchs, Y. Miao, CD80 on skin stem cells promotes local expansion of regulatory T cells upon injury to orchestrate repair within an inflammatory environment, Immunity 57 (2024) 1071, https://doi.org/10.1016/j.immuni.2024.04.003.
[81] E. Vergadi, E. Ieronymaki, K. Lyroni, K. Vaporidi, C. Tsatsanis, Akt signaling pathway in macrophage activation and M1/M2 polarization, J. Immunol. 198 (2017) 1006, https://doi.org/10.4049/jimmunol.1601515.
[82] F. Exposito, M. Redrado, M. Houry, K. Hastings, M. Molero-Abraham, T. Lozano, J.L. Solorzano, J. Sanz-Ortega, V. Adradas, R. Amat, E. Redin, S. Leon, N. Legarra, J. Garcia, D. Serrano, K. Valencia, C. Robles-Oteiza, G. Foggetti, N. Otegui, E. Felip, J.J. Lasarte, L. Paz-Ares, J. Zugazagoitia, K. Politi, L. Montuenga, A. Calvo, PTEN loss confers resistance to anti-PD-1 therapy in non-small cell lung cancer by increasing tumor infiltration of regulatory T cells, Cancer Res. 83 (2023) 2513, https://doi.org/10.1158/0008-5472.
[83] J.M. Moreau, M. Velegraki, C. Bolyard, M.D. Rosenblum, Z. Li, Transforming growth factor-β1 in regulatory T cell biology, Sci Immunol. 7 (2022) eabi4613, https://doi.org/10.1126/sciimmunol.abi4613.
[84] I. Kimiz-Gebologlu, S.S. Oncel, Exosomes: large-scale production, isolation, drug loading efficiency, and biodistribution and uptake, J Control Release 347 (2022) 533, https://doi.org/10.1016/j.jconrel.2022.05.027.
[85] D.M. Pegtel, S.J. Gould, Exosomes. Annu Rev Biochem. 88 (2019) 487, https://doi.org/10.1146/annurev-biochem-013118-111902.
[86] R. Kumar, Q. Tang, S.A. Müller, P. Gao, D. Mahlstedt, S. Zampagni, Y. Tan, A. Klingl, K. Bötzel, S.F. Lichtenthaler, G.U. Höglinger, T. Koeglsperger, Fibroblast growth factor 2-mediated regulation of neuronal exosome release depends on VAMP3/cellubrevin in hippocampal neurons, Adv. Sci. 7 (2020) 1902372, https://doi.org/10.1002/advs.201902372.
[87] P. Adhikari, T.E. Ayo, J.C. Vines, S. Sugita, H. Xu, Exocytic machineries differentially control mediator release from allergen-triggered RBL-2H3 cells, Inflamm. Res. 72 (2023) 639, https://doi.org/10.1007/s00011-023-01698-z.
[88] A. Avila, A.J. Acuña, M.T. Do, L.T. Samuel, A.F. Kamath, Intra-articular injection receipt within 3 months prior to primary total knee arthroplasty is associated with increased periprosthetic joint infection risk, Knee Surg. Sports Traumatol. Arthrosc. 30 (2022) 4088, https://doi.org/10.1007/s00167-022-06942-3.
[89] I. Usach, R. Martinez, T. Festini, J.E. Peris, Subcutaneous injection of drugs: literature review of factors influencing pain sensation at the injection site, Adv. Ther. 36 (2019) 2986, https://doi.org/10.1007/s12325-019-01101-6.
[90] C. Tu, H. Lu, T. Zhou, W. Zhang, L. Deng, W. Cao, Z. Yang, Z. Wang, X. Wu, J. Ding, F. Xu, C. Gao, Promoting the healing of infected diabetic wound by an anti-bacterial and nano-enzyme-containing hydrogel with inflammation-suppressing, ROS-scavenging, oxygen and nitric oxide-generating properties, Biomaterials 286 (2022) 121597, https://doi.org/10.1016/j.biomaterials.2022.121597.
[91] Y. Zou, J. Hu, W. Huang, S. Ye, F. Han, J. Du, M. Shao, R. Guo, J. Lin, Y. Zhao, Y. Xiong, X. Wang, Non-mitogenic fibroblast growth factor 1 enhanced angiogenesis following ischemic stroke by regulating the sphingosine-1-phosphate 1 pathway, Front. Pharmacol. 11 (2020) 59, https://doi.org/10.3389/fphar.2020.00059.
[92] C. Fan, Y. Oduk, M. Zhao, X. Lou, Y. Tang, D. Pretorius, M.T. Valarmathi, G. P. Walcott, J. Yang, P. Menasche, P. Krishnamurthy, W. Zhu, J. Zhang, Myocardial protection by nanomaterials formulated with CHIR99021 and FGF1, JCI Insight 5 (2020) e132796, https://doi.org/10.1172/jci.insight.132796.
[93] C. Wang, M. Wang, T. Xu, X. Zhang, C. Lin, W. Gao, H. Xu, B. Lei, C. Mao, Engineering bioactive self-healing antibacterial exosomes hydrogel for promoting chronic diabetic wound healing and complete skin regeneration, Theranostics 9 (2019) 65, https://doi.org/10.7150/thno.29766.
[94] K.R. Olumesi, D.J. Goldberg, A review of exosomes and their application in cutaneous medical aesthetics, J. Cosmet. Dermatol. 22 (2023) 2628, https://doi.org/10.1111/jocd.15930.
[95] I. Ludolph, A. Cai, A. Arkudas, W. Lang, U. Rother, R.E. Horch, Indocyanine green angiography and the old question of vascular autonomy - long term changes of microcirculation in microsurgically transplanted free flaps, Clin. Hemorheol. Microcirc. 72 (2019) 421–430, https://doi.org/10.3233/CH-180544.
[96] C. Deng, K. Dong, Y. Liu, K. Chen, C. Min, Z. Cao, P. Wu, G. Luo, G. Cheng, L. Qing, J. Tang, Hypoxic mesenchymal stem cell-derived exosomes promote the survival of skin flaps after ischaemia-reperfusion injury via mTOR/ULK1/FUNDC1 pathways, J Nanobiotechnology 21 (2023) 340, https://doi.org/10.1186/s12951-023-02098-5.
[97] Y. Bai, Y.D. Han, X.L. Yan, J. Ren, Q. Zeng, X.D. Li, X.T. Pei, Y. Han, Adipose mesenchymal stem cell-derived exosomes stimulated by hydrogen peroxide enhanced skin flap recovery in ischemia-reperfusion injury, Biochem. Biophys. Res. Commun. 500 (2018) 310, https://doi.org/10.1016/j.bbrc.2018.04.065.
[98] Q. Niu, Y. Yang, D. Li, W. Guo, C. Wang, H. Xu, Z. Feng, Z. Han, Exosomes derived from bone marrow mesenchymal stem cells alleviate ischemia-reperfusion injury

and promote survival of skin flaps in rats, Life 12 (2022) 1567, https://doi.org/10.3390/life12101567.

[99] C.M. Pu, C.W. Liu, C.J. Liang, Y.H. Yen, S.H. Chen, Y.F. Jiang-Shieh, C.L. Chien, Y. C. Chen, Y.L. Chen, Adipose-derived stem cells protect skin flaps against ischemia/reperfusion injury via IL-6 expression, J. Invest. Dermatol. 137 (2017) 1353, https://doi.org/10.1016/j.jid.2016.12.030.

[100] X. Shi, G. Yang, M.Y. Liu, M.T. Yuan, D. Wang, X.F. Wang, Exosomes derived from human dental pulp stem cells increase flap survival with ischemia-reperfusion injuries, Regen. Med. 18 (2023) 313, https://doi.org/10.2217/rme-2022-0206.

[101] M. Pomatto, C. Gai, F. Negro, M. Cedrino, C. Grange, E. Ceccotti, G. Togliatto, F. Collino, M. Tapparo, F. Figliolini, T. Lopatina, M.F. Brizzi, G. Camussi, Differential therapeutic effect of extracellular vesicles derived by bone marrow and adipose mesenchymal stem cells on wound healing of diabetic ulcers and correlation to their cargoes, Int. J. Mol. Sci. 22 (2021) 3851, https://doi.org/10.3390/ijms22083851.

[102] D. Wang, C. Zhao, F. Xu, A. Zhang, M. Jin, K. Zhang, L. Liu, Q. Hua, J. Zhao, J. Liu, H. Yang, G. Huang, Cisplatin-resistant NSCLC cells induced by hypoxia transmit resistance to sensitive cells through exosomal PKM2, Theranostics 11 (2021) 2860, https://doi.org/10.7150/thno.51797.

[103] C.A. Downs, V.D. Dang, N.M. Johnson, N.D. Denslow, A.A. Alli, Hydrogen peroxide stimulates exosomal cathepsin B regulation of the receptor for advanced glycation end-products (RAGE), J. Cell. Biochem. 119 (2018) 599, https://doi.org/10.1002/jcb.26219.